

**Linear correlations of Gibbs free energy for rare earth element oxide,
hydroxide, chloride, fluoride, carbonate, and ferrite minerals and crystalline
solids**

Ruiguang Pan^a, Chen Zhu^{a,*}

^aDepartment of Earth and Atmospheric Sciences, Indiana University Bloomington,
Bloomington, IN 47405, USA

*Corresponding authors:

C. Zhu: E-mail address: chenzhu@indiana.edu; ORCID ID #: 0000-0001-5374-6787

Abstract

Rare Earth Elements (REE) are critical minerals (metals) for the transition from fossil fuels to renewable and clean energy. Accurate thermodynamic properties of REE minerals and other crystalline solids are crucial for geochemical modeling of the solubility, speciation, and transport of REE in ore formation, extraction, chemical processing, and recycling processes. However, the Gibbs free energies of formation ($\Delta G_{f, \text{REEX}}^{\circ}$) for these solids from different sources vary by 10s kJ/mol. We applied the Sverjensky linear free energy relationship (LFER) to evaluate their internal consistency and predict the unavailable ΔG_f° of the REE solids. By considering both the effects of ionic radius size and corresponding aqueous ion properties, the Sverjensky LFER,

$$\Delta G_{f, \text{REEX}}^{\circ} - \beta_{\text{REEX}} r_{\text{REE}^{Z+}} = a_{\text{REEX}} \Delta G_{n, \text{REE}^{Z+}}^{\circ} + b_{\text{REEX}}$$

allows estimates with much accuracy and precision. Here, $r_{\text{REE}^{Z+}}$ represents the Shannon-Prewitt ionic radii (\AA) of REE^{Z+} , and $\Delta G_{n, \text{REE}^{Z+}}^{\circ}$ denotes the non-solvation contribution to the ΔG_f° of the aqueous REE^{Z+} ion. X represents the remainder of the compounds. In this study, the parameters a_{REEX} , b_{REEX} , and β_{REEX} were regressed from ΔG_f° compilations in the literature for 13 isostructural families. Based on these linear relationships, we recommend a set of internally consistent $\Delta G_{f, \text{REEX}}^{\circ}$ for 119 end-members of REE oxides, hydroxides, chlorides, fluorides, carbonates, hydrous carbonates, and ferrites. These $\Delta G_{f, \text{REEX}}^{\circ}$ are combined with experimental or predicted values of S° , V° , and Cp° from the literature and incorporated into a new SUPCRT database, which allows the calculations of thermodynamic properties to high P - T conditions (e.g., up to 1000 °C and 5 kb). The $\log K_{\text{sp}}$ of REE solid dissociation reactions were incorporated into a modified USGS program PHREEQC for calculations of speciation, solubility, and reactive transport. These thermodynamic databases will also be incorporated into the MINES database to be used together with the GEMS code package in the future.

Keywords: REE minerals; linear correlations; Gibbs free energy; Internal consistency; Thermodynamic database

1. Introduction

Rare earth elements (REE) minerals are critical minerals (metals) typically incorporated into a large variety of complex phases to provide tailored mechanical, electrical, optical, and magnetic properties. They are critical metals used for renewable energy to develop a green economy (Goodenough et al., 2018; Grandell et al., 2016). Thermodynamic properties of rare earth mineral materials control their phase stability, material compatibility, corrosion, and transformation (Migdisov et al., 2016; Navrotsky et al., 2015; Pan et al., 2024b). Therefore, accurate thermodynamic properties of those REE minerals will enhance our understanding of the chemical processes related to the formation of these REE minerals or solids, including extraction, processing, and recycling processes (Iloje et al., 2019; Migdisov et al., 2019; Pan et al., 2024a; Zhang et al., 2016). Even though the thermodynamic properties (e.g., ΔG_f° , ΔH_f° , and S° , symbol definitions can be found in Table 1) of REE minerals have been experimentally determined (e.g., calorimetry, etc.), the reported thermodynamic properties (e.g., Gibbs free energies of formation, ΔG_f°) of those mineral end-members from different sources vary greatly. Figure 1 shows the comparisons of standard state ΔG_f° for cubic $\text{Er}(\text{OH})_3$ and CeO_2 end-members, which vary up to 35 kJ mol^{-1} .

Linear correlation of ΔG_f° values in an isostructural family of crystalline solids is a way of evaluating the internal consistency of ΔG_f° values of the end-members. Sverjensky and Molling (1992) pioneered an empirical linear free energy correlation for crystalline solids within the same structure families. This linear correlation has been successfully applied to isostructural families including REE phosphates (Pan et al., 2024a), and carbonates, pyrochlore, zirconolite, and uranate (MUO_4) minerals (Wang and Xu, 1999, 2001; Xu and Wang, 1999a, b, c). The linear correlation was also used to calculate the metal partitioning between carbonate minerals and solutions (Wang and Xu, 2001) and surface precipitation constants for the sorption (Zhu, 2002). The REEs are chemically very similar to each other, showing similar crystal-chemical and solution-chemical properties (Migdisov et al., 2016). For this study, our objectives are to, first, test if the linear relationships in Sverjensky and Molling (1992) are applicable to the experimentally derived ΔG_f° values of the trivalent and tetravalent REE minerals and, second, recommend a set of internally consistent thermodynamic database for those REE solids after evaluation of their internal consistency. Although not all REE crystalline solids reviewed in this

study are minerals, we do not always say “REE minerals and other crystalline solids” to avoid cumbersomeness.

2. Formulation of the linear free energy correlation

In this study, we applied the linear free energy correlation for isostructural families proposed by [Sverjensky and Molling \(1992\)](#) to REE mineral end-members REEX, which individually share the same isostructural crystal structure with trivalent and tetravalent cations. We generally follow the procedure in [Sverjensky and Molling \(1992\)](#) to derive the linear correlations of the ΔG_f^o of the isostructural REE mineral families. A list of symbols and definitions is provided in [Table 1](#). Some ΔG_f^o values of the actinide mineral end-members were used to assist in constructing the linear correlations.

The $\Delta G_{n, \text{REE}^{Z+}}^o$ non-solvation contribution to the Gibbs energy of formation (ΔG_f^o) of the REE^{Z+} ions were calculated as:

$$\Delta G_{n, \text{REE}^{Z+}}^o = \Delta G_{f, \text{REE}^{Z+}}^o - \Delta G_{s, \text{REE}^{Z+}}^o \quad (1)$$

where $\Delta G_{s, \text{REE}^{Z+}}^o$ refers to the solvation contribution to the Gibbs energy of formation (ΔG_f^o , REE^{Z+}) of the aqueous REE^{Z+} ions. $\Delta G_{s, \text{REE}^{Z+}}^o$ can be calculated from the following equation:

$$\Delta G_{s, \text{REE}^{Z+}}^o = \omega_{\text{REE}^{Z+}} \left(\frac{1}{\varepsilon} - 1 \right) \quad (2)$$

where $\omega_{\text{REE}^{Z+}}$ denotes the conventional Born solvation coefficient for the aqueous ion REE^{Z+} and ε refers to the dielectric constant of water, which is 78.47 at 25 °C and 1 bar ([Fernández et al., 1995](#)). The value of $\omega_{\text{REE}^{Z+}}$ can be calculated from:

$$\omega_{\text{REE}^{Z+}} = \omega_{\text{REE}^{Z+}}^{\text{abs}} - Z \cdot \omega_{\text{H}^+}^{\text{abs}} \quad (3)$$

where $\omega_{\text{H}^+}^{\text{abs}}$ equals $2.254 \times 10^5 \text{ J mol}^{-1}$ ([Shock and Helgeson, 1988](#)); $\omega_{\text{REE}^{Z+}}^{\text{abs}}$ refers to the absolute Born coefficient of the aqueous REE^{Z+} ion, which can be further derived:

$$\omega_{\text{REE}^{Z+}}^{\text{abs}} = (6.94657 \times 10^5) \cdot Z^2 / (r_{e, \text{REE}^{Z+}}) \quad (4)$$

where $r_{e, \text{REE}^{Z+}}$ denotes the effective electrostatic radius of the aqueous REE^{Z+} ion, which can be obtained from the following equation:

$$r_{e, \text{REE}^{Z+}} = r_{\text{REE}^{Z+}} + Z(0.94) \quad (5)$$

where $r_{\text{REE}^{Z+}}$ refers to the crystallographic radius of the aqueous REE^{Z+} ion, which represents its Shannon-Prewitt radius (Å) (Shannon and Prewitt, 1969) (Table 2). Z in Eqs. 3–5 represents the charge of the aqueous REE^{Z+} , which is 3^+ for trivalent ions and 4^+ for tetravalent ions.

The above equations were used to calculate values of ΔG_n^o (Table 2) for the metal aqueous REE^{Z+} cations. To present more clearly its linear correlation for $\Delta G_{f, \text{REEX}}^o$, $\Delta G_{n, \text{REE}^{Z+}}^o$, and $r_{\text{REE}^{Z+}}$, we expressed the equation as below and plotted the left-hand side of Eqs. (6 and 7) against the aqueous cation parameter $\Delta G_{n, \text{REE}^{Z+}}^o$,

$$\Delta G_f' = a_{\text{REEX}} \cdot \Delta G_{n, \text{REE}^{Z+}}^o + b_{\text{REEX}} \quad (6)$$

$$\Delta G_f' = \Delta G_{f, \text{REEX}}^o - \beta_{\text{REEX}} \cdot r_{\text{REE}^{Z+}} \quad (7)$$

where REEX refers to the isostructural family of REE solids. $\Delta G_{f, \text{REEX}}^o$ refers to the standard Gibbs free energy of formation for REEX. The parameters a_{REEX} , b_{REEX} , and β_{REEX} are regression parameters for the isostructural family of REE minerals.

3. Data availability

Table 2 lists the REE^{Z+} crystallographic radii r , ΔG_n^o non-solvation contributions to the ΔG_f^o of the aqueous REE^{Z+} ions, and ΔG_f^o of the REE end-members which are needed to carry out the regression of the free energy linear correlation.

3.1. REE^{Z+} ion parameters ($Z = 3$ or 4)

REE elements occur naturally in the trivalent state but can be also in divalent (e.g., Eu) and tetravalent states (e.g., Ce, Pr, and Tb) (Atwood, 2013). Here, $Z = 4$ is for (Ce, Pr, and Tb) O_2 , and $Z = 3$ is for all other REE minerals. The crystallographic radii of the REE^{Z+} ions are needed to perform the regression of the linear free energy correlations. For REE oxides, REE^{3+} ions in REE oxide have 7- (A-Type) and 6- (B- and C-Type) fold coordination numbers (Cordfunke and Konings, 2001). REE^{4+} ion in REEO_2 oxide has 8-fold coordination numbers. For REE hydroxides, REE^{3+} ions in $\text{REE}(\text{OH})_3$ solids have 9-fold coordination numbers. REE^{3+} ions in REE chlorides with UCl_3 and AlCl_3 crystal structures have 9- and 6-fold coordination numbers, respectively (Cotton, 2024). REE^{3+} ions in REE fluorides have 9-fold coordination numbers (Cotton, 2024). REE^{3+} ions in both carbonates ($\text{REE}_2(\text{CO}_3)_3$) and hydrous carbonates ($\text{REE}_2(\text{CO}_3)_3 \cdot 3\text{H}_2\text{O}$) have 6-fold coordination numbers. REE^{3+} ions in perovskite ferrites

(REEFeO₃) and zirconates (REE₂Zr₂O₇) have 12- and 8-fold coordination numbers, respectively. Detailed REE^{Z+} ion parameters can be found in [Table 2](#). The REE^{Z+} crystallographic radius varies with the numbers of their coordination state. In this study, the REE^{Z+} crystallographic radii ($r_{\text{REE}^{Z+}}$) at different coordination numbers were taken from [Shannon \(1976\)](#) and a machine learning study by [Baloch et al. \(2021\)](#). The ΔG_f° of REE^{Z+} aqueous ions are from [Shock and Helgeson \(1988\)](#), which can be found in [Table 2](#). ΔG_n° values were derived from Eqs. 1–7 and can be found in [Table 2](#).

3.2. REE mineral thermodynamic parameters

REE mineral end-members show slightly different crystal structures due to their different atomic sizes and atom arrangement. For example, A-Type, B-Type, and C-Type REE oxide end-members (REE₂O₃) exhibit hexagonal, monoclinic, and cubic structures, respectively ([Cordfunke and Konings, 2001](#)). The molar volumes for the end-members of REE oxides were calculated from the unit cell parameters as listed in [Table 2](#). The molar volumes of non-experimentally measured and hypothetical end-members were calculated from the correlation of the REE oxide isostructural families. The volume correlations are shown in Appendix A.

ΔG_f° values at 25 °C and 1 bar of the REE oxide end-members were from the review study of [Konings et al. \(2014\)](#). The ΔG_f° of REE hydroxides are from the recommendation of [Navrotsky et al. \(2015\)](#). The ΔG_f° of REE chlorides are from [Konings and Kovács \(2003\)](#). The ΔG_f° of REE fluorides are from the solubility experiments from [Migdisov et al. \(2009\)](#). The ΔG_f° of REE carbonates are from [Navrotsky et al. \(2015\)](#) and [Smith and Martell \(1976\)](#). The ΔG_f° of hydrous REE carbonates are from the calculated results from [Karapet'yants et al. \(1977\)](#). The ΔG_f° of REE perovskite are from the recommendation of [Navrotsky et al. \(2015\)](#). The ΔG_f° of REE zirconates are from [Navrotsky et al. \(2015\)](#) and [Helean et al. \(2001\)](#). The detailed ΔG_f° of REE minerals can be found in [Table 2](#), and their reference source can be found in the legends of the figures for the constructed linear correlations. The ΔG_f° values from other studies ([Konings et al., 2014](#); [Migdisov et al., 2016](#); [Navrotsky et al., 2015](#)) are also included in the discussion to compare against the results retrieved or evaluated from the linear correlation study.

4. Results

4.1. REE oxides (REE₂O₃ and REEO₂)

In this study, we only cover the most common REE oxides (REE₂O₃ and REEO₂) with REE charges in 3+ and 4+. The free energies of the REE oxides within the same isostructural family were regressed using Eqs. 6 and 7, together with the values of REE ionic radii and ΔG_n^o from Table 2. The regression results for the four isostructural families are summarized in Table 3 and plotted in Fig. 2. The results show that the linear correlation lines of A-Type, B-Type, C-Type REE₂O₃, and cubic REEO₂ have R² values of 0.9995, 0.9993, 0.9970, and 0.9931, respectively, indicating excellent linear relationships for those selected thermodynamic parameters. The linear free energy relationships can be expressed as:

$$\Delta G_{f,A-Type}^o - 732.39 r_{\text{REE}^{3+}} = 0.7422 G_{n,\text{REE}^{3+}}^o - 2674.67 \quad (8)$$

$$\Delta G_{f,B-Type}^o - 819.51 r_{\text{REE}^{3+}} = 1.9899 G_{n,\text{REE}^{3+}}^o - 3120.24 \quad (9)$$

$$\Delta G_{f,C-Type}^o - 1258.34 r_{\text{REE}^{3+}} = 2.2599 G_{n,\text{REE}^{3+}}^o - 3647.73 \quad (10)$$

$$\Delta G_{f,Cubic}^o - 19.389 r_{\text{REE}^{4+}} = 0.6045 G_{n,\text{REE}^{4+}}^o - 1599.64 \quad (11)$$

where the symbols are defined in Table 1. The ΔG_f^o of the metastable forms (A-Type Pm₂O₃, and C-Type Pm₂O₃, Sm₂O₃, and Eu₂O₃) of REE oxide end-members were predicted from the correlations as well to study the phase transition thermodynamic behaviors at elevated temperatures.

The differences between experimental and calculated values of the Gibbs free energies of the formation of the solids are shown in Fig. 3. The discrepancy between calculated and experimental Gibbs free energies is less than 8 kJ mol⁻¹. The discrepancies are 15 kJ mol⁻¹ for B-Type Pm₂O₃, which are not used in the linear regressions. These uncertainties (<8 kJ mol⁻¹) are within those reported from calorimetric experiments (~<10 kJ mol⁻¹) (Fig. 3). The linear correlations for B- and C-Type REE₂O₃ are generally parallel (Fig. 2). These results indicate that the regressed linear correlations closely fit the experimentally derived ΔG_f^o of isostructural families of the four types of REE oxides.

For REE oxides, including some actinide oxides, their thermodynamic parameters have been reviewed by Konings et al. (2014). For the REE₂O₃ with A, B, and C-Type structures, we still recommend using the ΔG_f^o of minerals from Konings et al. (2014) and the recommended values for the predicted end-members in this study (Fig. 2) due to the excellent linear correlation

(Fig. 2a). The ΔH_f° of the REE_2O_3 and REEO_2 have been assessed by Cordfunke and Konings (2001) and directly accepted by Konings et al. (2014). To calculate the ΔS_f° of REE oxides, we selected the S° of these REE metals from Konings and Beneš (2010), and the S° value (205.15 J mol⁻¹ K⁻¹) of O₂ (g) from Robie et al. (1978).

For A-Type REE_2O_3 , the recommended ΔG_f° of minerals shows consistent values with the previous studies (Baker and Holley, 1968; Fitzgibbon et al., 1973; Fitzgibbon et al., 1968; Huber Jr and Holley Jr, 1952; Justice and Westrum Jr, 1963; Montgomery and Hubert, 1959; Popova and Monaenkova, 1989) within the presented errors as in Fig. 2a. The reported ΔG_f° values of minerals in Mah (1961); Schumm et al. (1973); Spedding and Miller (1952) are much higher than the recommendation. However, these values in Cordfunke and Konings (2001); Fitzgibbon et al. (1965); Hennig and Oppermann (1998); Huntelaar et al. (2000); (Kuznetsov et al., 1960); Morss et al. (1989); Oppermann et al. (1997); Putnam et al. (2000); Stubblefield et al. (1956) are significantly smaller than the recommended values in this study (Fig. 2a). For B-Type REE_2O_3 , the recommended ΔG_f° values of minerals are consistent with most of previous studies (Baker et al., 1972; Cordfunke and Konings, 2001; Fitzgibbon et al., 1972; Gvelesiani and Yashvili, 1967; Hennig and Oppermann, 1997; Huber Jr et al., 1964; Huber Jr et al., 1955; Schumm et al., 1973), but showing a higher value than the ΔG_f° of Eu_2O_3 (B-Type) from Hennig and Oppermann (1998) and a much lower value than the ΔG_f° of Sm_2O_3 (B-Type) from Spedding (1959). For C-Type REE_2O_3 , the recommended ΔG_f° values of minerals in this study are consistent with most of the previous studies (Huber Jr et al., 1956b, 1957; Huber Jr and Holley Jr, 1952), only showing higher ΔG_f° values of Y_2O_3 (C-Type) and Er_2O_3 (C-Type) than Morss et al. (1993) and higher ΔG_f° values of Er_2O_3 (C-Type) than Huber Jr et al. (1956a); Stuve (1965). For cubic REEO_2 , the recommended ΔG_f° values of minerals are consistent with the previous studies (Fitzgibbon et al., 1973; Gruber et al., 2002; Johnson et al., 1969; Justice and Westrum Jr, 1969; Morss and Konings, 2004; Schumm et al., 1973), and only showing an average ΔG_f° value of AmO_2 from Eyring et al. (1952) and the recommended value from Konings et al. (2014), and a lower ΔG_f° value of UO_2 than the recommended value from Konings et al. (2014).

4.2. REE hydroxides ($\text{REE}(\text{OH})_3$)

REE hydroxides with $\text{REE}(\text{OH})_3$ composition only exhibit one cubic crystal structure. The free energies of the REE hydroxides within the same isostructural family were regressed as

Eq. 12, using the values of REE ionic radii and ΔG_n^o from Table 2. The regression results for this isostructural family are summarized in Table 3 and plotted in Fig. 4a.

$$\Delta G_{f, \text{REE}(\text{OH})_3}^o + 530.0 r_{\text{REE}^{3+}} = 1.070 G_{n, \text{REE}^{3+}}^o - 2122.19 \quad (12)$$

In the linear correlation calculation, we didn't use the ΔG_f^o values of hydroxide-(Dy, Er, and Y) due to significant deviations from the constructed linear line (Fig. 5a). Moreover, we predicted the ΔG_f^o of hydroxide-(Pm and Lu) using the calculated linear correlation (Eq. 12). The calculated linear correlation shows an excellent R^2 value of 0.9944 (Table 3). The differences between experimental and calculated values of the ΔG_f^o for REE-hydroxides are shown in Fig. 4b. The discrepancy between calculated and experimental ΔG_f^o is less than 6.0 kJ mol⁻¹. These uncertainties are within those reported from calorimetric experiments in the literature (<10 kJ mol⁻¹) (Fig. 4). These results indicate that the regressed linear correlations closely fit the experimentally derived ΔG_f^o of isostructural families of REE hydroxides (Fig. 4a).

For REE hydroxides, Navrotsky et al. (2015) reviewed previously reported thermodynamic parameters, and most of the ΔH_f^o recommended by Navrotsky et al. (2015) are from Diakonov et al. (1998), as they show similar ΔG_f^o - βr values in Fig. 4a. The recommended ΔG_f^o from Navrotsky et al. (2015) show close values with the study of Brookins (1988) but overall slightly smaller than the dataset from Ragavan and Adams (2009) and Rossini (1961). The ΔG_f^o of Eu(OH)₃ from Ragavan and Adams (2009) is extremely smaller than all others (Fig. 4a).

4.3. REE chlorides (REEC1₃)

REE chlorides show two types of crystal structures, UCl₃ structure for (La to Gd)Cl₃ and AlCl₃ structure for (Dy to Lu and Y)Cl₃. TbCl₃ shows a unique crystal structure of PuBr₃ with Tb having a coordination number of 8 (Cotton, 2024). The free energies of the REE chlorides within the same isostructural family were regressed using the values of REE ionic radii and ΔG_n^o from Table 2. The linear correlations for the REE chlorides with UCl₃ and AlCl₃ crystal structures are described in Eqs. 13 and 14, respectively. The regression results for this isostructural family are summarized in Table 3 and have been plotted in Fig. 5a.

$$\Delta G_{f, \text{REEC1}_3}^o + 75.01 r_{\text{REE}^{3+}} = 1.013 G_{n, \text{REE}^{3+}}^o - 1268.1 \quad (13)$$

$$\Delta G_{f, \text{REEC1}_3}^o + 309.19 r_{\text{REE}^{3+}} = 1.017 G_{n, \text{REE}^{3+}}^o - 1603.73 \quad (14)$$

In the linear correlation calculation, we used all the ΔG_f^o of REE chlorides with UCl_3 structure from [Konings and Kovács \(2003\)](#) but didn't use the ΔG_f^o of YCl_3 from this study due to the significant deviation from the constructed linear line ([Fig. 5a](#)). Therefore, ΔG_f^o of PmCl_3 and YCl_3 were predicted based on these linear correlations (Eqs. 13 and 14). Because the TbCl_3 end-member has a unique crystal structure, which is neither UCl_3 nor AlCl_3 , we directly accepted the ΔG_f^o value ($-1010.6 \text{ kJ mol}^{-1}$) from [Konings and Kovács \(2003\)](#). The calculated linear lines show excellent R^2 values of 0.9985 and 0.9830, for REE chlorides with UCl_3 and AlCl_3 structures, respectively ([Table 3](#)). The differences between experimental and calculated values of the ΔG_f^o of REE-chlorides are shown in [Fig. 5b](#). The discrepancy between calculated and experimental ΔG_f^o is less than 4.0 kJ mol^{-1} ([Fig. 5b](#)). For REE chlorides, the constructed linear correlations for the two structures of isostructural families show excellent linear correlations using the ΔG_f^o values from [Konings and Kovács \(2003\)](#), except YCl_3 .

4.4. REE fluorides (REEF_3)

REE fluorides show two types of crystal structures, LaF_3 structure for $(\text{La to Nd})\text{F}_3$ and YF_3 structure for $(\text{Sm to Lu and Y})\text{F}_3$. The free energies of the REE fluorides within the same isostructural families from solubility experiments ([Migdisov et al., 2009](#)) were regressed ([Fig. 6](#)), using the values of REE ionic radii and ΔG_n^o from [Table 2](#). The regression results for these isostructural families are summarized in [Table 3](#) and plotted in [Fig. 6a](#). The linear correlations for the REE fluorides with LaF_3 and YF_3 crystal structures are described by Eq. 15 and 16, respectively.

$$\Delta G_{f,\text{REEF}_3}^o + 78.29 r_{\text{REE}^{3+}} = 0.5665 G_{n,\text{REE}^{3+}}^o - 1844.46 \quad (15)$$

$$\Delta G_{f,\text{REEF}_3}^o + 174.66 r_{\text{REE}^{3+}} = 0.867 G_{n,\text{REE}^{3+}}^o - 2021.58 \quad (16)$$

In the linear correlation calculation, we used all the ΔG_f^o of REE fluorides with LaF_3 structure from [Migdisov et al. \(2016\)](#) ([Fig. 6a](#)). ΔG_f^o of EuF_3 and YF_3 were not reported in [Migdisov et al. \(2016\)](#), and therefore were predicted in this study based on Eq. 16. The calculated linear correlations show excellent R^2 values of 0.99750 and 0.9909, for REE fluorides with LaF_3 and YF_3 crystal structures, respectively ([Table 3](#)). The differences between experimental and calculated values of the ΔG_f^o of REE fluorides are shown in [Fig. 6b](#). For all of the 13 points selected, the discrepancies between calculated and experimental ΔG_f^o values are

less than 8.0 kJ mol⁻¹ for the LaF₃ isostructural family and less than 3 kJ mol⁻¹ for the LaF₃ isostructural family. These results indicate that the regressed linear correlations closely fit the ΔG_f^o derived from the solubility of REE fluorides. The ΔG_f^o dataset of REE fluorides from calorimetric experiments was calculated from the ΔH_f^o and S^o of REE fluorides reported by [Konings and Kovács \(2003\)](#), the S^o of REE metals from [Konings and Beneš \(2010\)](#), and the S^o (205.15 J mol⁻¹ K⁻¹) of F₂(g) from [Robie et al. \(1978\)](#). This ΔG_f^o dataset of REE fluorides does not fall on these linear lines. The constructed correlations using the ΔG_f^o values from the solubility data ([Migdisov et al., 2016](#); [Migdisov et al., 2009](#)) show much better correlations than those from [Konings and Kovács \(2003\)](#).

4.5. REE carbonates (REE₂(CO₃)₃) and hydrous carbonates (REE₂(CO₃)₃·nH₂O)

REE carbonates only show one crystal structure (REE₂(CO₃)₃), and hydrous REE carbonates have three crystal structures distinguished by H₂O contents, as (La-Nd)₂(CO₃)₃·8H₂O, (Sm-Tm, and Y)₂(CO₃)₃·6H₂O, and (Yb and Lu)₂(CO₃)₃·3H₂O. The free energies of the REE carbonates and hydrous carbonates within their individual isostructural family were regressed using the values of REE ionic radii and ΔG_n^o from [Table 2](#). Due to the limited experiments on the reported ΔG_f^o of REE carbonates, we added available isostructural actinide (Am, Np, U, and Pu) carbonates to obtain a better constrained linear correlation ([Fig. 7](#)). The regression results for these isostructural families are summarized in [Table 3](#) and plotted in [Figs. 7a](#) and [8a](#).

$$\Delta G_{f, \text{REE}_2(\text{CO}_3)_3}^o + 948.34 r_{\text{REE}^{3+}} = 2.098 G_{n, \text{REE}^{3+}}^o - 4640.35 \quad (17)$$

$$\Delta G_{f, \text{REE}_2(\text{CO}_3)_3 \cdot 8\text{H}_2\text{O}}^o + 281.58 r_{\text{REE}^{3+}} = 1.227 G_{n, \text{REE}^{3+}}^o - 5002.35 \quad (18)$$

$$\Delta G_{f, \text{REE}_2(\text{CO}_3)_3 \cdot 3\text{H}_2\text{O}}^o + 616.03 r_{\text{REE}^{3+}} = 2.0416 G_{n, \text{REE}^{3+}}^o - 4946.65 \quad (19)$$

In the linear correlation calculation, we used the reported ΔG_f^o of REE carbonates from [Navrotsky et al. \(2015\)](#) and [Smith and Martell \(1976\)](#), and actinide carbonates from [OECD \(1985\)](#). We didn't use the ΔG_f^o of Nd carbonate from [Navrotsky et al. \(2015\)](#) due to the significant deviation from the constructed linear line ([Fig. 7a](#)). Therefore, ΔG_f^o of non-experimentally measured REE carbonates are predicted based on the linear correlations in Eq. 17 and plotted in [Fig. 7a](#). The calculated linear line of REE carbonate shows an excellent R² value of 0.9988 ([Table 3](#)). The differences between experimental and calculated ΔG_f^o values for REE carbonates are less than 6.0 kJ mol⁻¹ ([Fig. 7b](#)). For REE carbonates, the constructed linear

correlation agrees with most of the reported ΔG_f^o values from (Brookins, 1983) except that the (Gd, Tm, and Lu)₂(CO₃)₃ show higher ΔG_f^o values.

For hydrous REE carbonates, we constructed the linear correlations for (La-Nd)₂(CO₃)₃·8H₂O and (Sm-Tm, and Y)₂(CO₃)₃·3H₂O, but not for (Yb and Lu)₂(CO₃)₃·6H₂O because it only has two end-members, and they not applicable to the linear correlation method. For the selected ΔG_f^o of (La-Nd)₂(CO₃)₃·8H₂O, we still recommend using the existing ΔG_f^o of (Ce-Nd)₂(CO₃)₃·8H₂O because only four end-members are selected for the linear correlations. The ΔG_f^o value of La₂(CO₃)₃·8H₂O was therefore predicted. In terms of (Sm-Tm, and Y)₂(CO₃)₃·3H₂O, we didn't use the ΔG_f^o of (Tb and Y)₂(CO₃)₃·3H₂O due to their deviations from the linear correlation, so their ΔG_f^o values were also predicted in this study. The differences between the retrieved values from the experimental and calculated values are shown in Fig. 8b and c. Lastly, in terms of hydrous REE carbonates (Sm-Tm, and Y)₂(CO₃)₃·3H₂O and (Ce-Nd)₂(CO₃)₃·8H₂O, the discrepancies between the calculated and experimental ΔG_f^o values are less than 8.0 kJ mol⁻¹ (Fig. 8). For REE hydrous carbonates, the constructed linear correlation for REE₂(CO₃)₃·3H₂O structure family show an excellent linear correlation when using the only available estimated mineral ΔG_f^o values from Karapet'yants et al. (1977). The constructed linear correlation for REE₂(CO₃)₃·8H₂O structure family is fair due to the fact that this family only has four end-members. No linear correlation of ΔG_f^o values for (Yb and Lu)₂(CO₃)₃·6H₂O structure family because only two end-members exist.

4.6. REE perovskite ferrites (REEFeO₃)

The free energies of the REE perovskite ferrites within the same isostructural family were regressed using the values of REE ionic radii and ΔG_n^o from Table 2. REEFeO₃ crystalline solids only exhibit one crystal structure of perovskite. The regression results for this isostructural family are summarized in Table 3 and plotted in Fig. 10a.

$$\Delta G_{f, \text{REEFeO}_3}^o + 450.21 r_{\text{REE}^{3+}} = 0.9150 G_{n, \text{REE}^{3+}}^o - 2005.97 \quad (20)$$

In the linear correlation calculation, we used all the ΔG_f^o of REE perovskite ferrites from Navrotsky et al. (2015) but didn't use the ΔG_f^o of TmFeO₃ from their study due to the significant deviation from the constructed linear line (Fig. 6a). We therefore predicted the ΔG_f^o of (Tb, Tm, Yb, Ce, and Y)FeO₃, but we didn't predict the ΔG_f^o of (Er, Lu, and Pm)FeO₃ due to lack of radii data of those REE ions at coordination number of 12. The calculated linear correlation shows an

excellent R^2 value of 0.9878. The discrepancies between calculated and experimental ΔG_f^0 values are less than 8.0 kJ mol^{-1} for REE perovskite ferrites (Fig. 9b). For REE perovskite ferrites, the constructed linear correlation shows an excellent linear correlation, with only one end-member (TmFeO₃) deviating from the line (Fig. 9a). The thermodynamic parameters recommended by Navrotsky et al. (2015) are from Kaul et al. (1976) and Kanke and Navrotsky (1998).

4.7. REE zirconates (REE₂Zr₂O₇)

The free energies of the REE Zirconates within the same isostructural family were regressed using the values of REE ionic radii and ΔG_n^0 from Table 2. REE zirconates with REE₂Zr₂O₇ formula only exhibit one crystal structure of pyrochlore. The regression results for this isostructural family are summarized in Table 3 and plotted in Fig. 10. The regressed line has a negative slope (parameter a) which disagrees with other isostructural families that show positive slope values of the constructed correlation. The constructed linear correlation indicates that $\Delta G'_f$ has a negative correlation with the increasing ΔG_n^0 . Therefore, here we don't recommend using the dataset of ΔG_f^0 of REE zirconates from Navrotsky et al. (2015) and Gd₂Zr₂O₇ from Helean et al. (2000), as in Table 2.

5. Discussion

5.1. Comparisons between calorimetry and solubility-derived ΔG_f^0

Here, we compare the ΔG_f^0 values at 25 °C and 1 bar for end-members within an isostructural family derived from calorimetry and solubility experiments. Both calorimetry and solubility-derived ΔG_f^0 values generally follow a LFER trend, and it can be argued that these linear trends are parallel, but these trends are offset on the vertical axis by significant amounts. Recall that $\Delta G'_f = \Delta G_{f, \text{REEX}}^0 - \beta_{\text{REE}^{z+}}$. The volume effect of β_r is the same regardless of the experimental methods for measuring ΔG_f^0 . Therefore, the difference between the calorimetric and solubility-derived $\Delta G'_f$ resulted from ΔG_f^0 .

For REE fluorides, ΔG_f^0 from solubility data generally parallel with the calorimetric data but shows more negative values than the calorimetry data (Fig. 6). REE fluorides with the LaF₃ structure derived by the calorimetry data show a $\sim 28.8 \text{ kJ/mol}$ offset over solubility-derived ΔG_f^0 while REE fluorides with the YF₃ structure has a much smaller offset, $\sim 3.5 \text{ kJ/mol}$ compared to solubility-derived ΔG_f^0 . In terms of the solubility products $\log K_{\text{sp}}$ (e.g., REEF₃ = REE³⁺ + 3F⁻),

the offset in ΔG_f^0 with LaF_3 structure leads to a ~ 5.0 units more positive $\log K_{\text{sp}}$ at 25 °C and 1 bar. In other words, using the ΔG_f^0 values of (La, Ce, Pr, and Nd)-fluorides derived from calorimetric measurements, a geochemical model would predict that those fluorides are orders of magnitude more soluble than those using the solubility-derived ΔG_f^0 values at 25 °C and 1 bar in the literature. For REE fluorides with YF_3 structure, the small ~ 3.5 kJ/mol in ΔG_f^0 from these two measurements is within the error of chemometric experiments (~ 10 kJ/mol) and only leads to a ~ 0.6 unit more positive $\log K_{\text{sp}}$ at 25 °C and 1 bar.

Similar calorimetry-solubility discrepancies in ΔG_f^0 values at 25 °C and 1 bar were also found for xenotime. [Figure 11](#) shows an offset of ~ 22 kJ/mol between calorimetry and solubility-derived ΔG_f^0 but the offset is in the opposite direction as to fluorides. The solubility-derived ΔG_f^0 have more positive numbers. Using the calorimetry-derived ΔG_f^0 leads to 3.9 units lower in $\log K_{\text{sp}}$ for xenotime end-members, and therefore, predicting much lower xenotime solubility. On the other hand, for monazite, the calorimetry-derived ΔG_f^0 values at 25 °C and 1 bar agree with some solubility derived ΔG_f^0 values at 25 °C and 1 bar but not others ([Pan et al., 2024a](#)).

It is encouraging that both calorimetry- and solubility-derived ΔG_f^0 values typically fall along a linear trend, prescribed by the Sverjensky LFER, with solubility-derived values having excellent linear correlations while calorimetry-derived values are more scattered. To resolve these discrepancies is important but this work is beyond the scope of the current study, and we will endeavor in the future to resolve them.

5.2. Consistency between ΔG_f^0 for aqueous REE ions and REE crystalline solids

[Sverjensky and Molling \(1992\)](#) pointed out “A second way to use our linear free energy equation is to predict the standard Gibbs free energies of formation of aqueous cations at 25 °C and 1 bar when only the free energies of the solids are known. This is particularly useful for highly charged aqueous cations ($Z = 3$ or 4)” In other words, the LFER established in this study and [Pan et al. \(2024a\)](#) for 16 isostructural families provide a dataset to evaluate the internal consistency of the ΔG_f^0 of aqueous REE ions as well. For the 16 linear correlations ([Figs. 2-10](#), and those in [Pan et al. \(2024a\)](#)), the ΔG_f^0 of aqueous REE ions (REE^{3+} , Ce^{4+} , Pr^{4+} , and Tb^{4+}) are all from [Shock et al. \(1997\)](#) and [Shock and Helgeson \(1988\)](#), which are internally consistent ([Table 2](#)). Alternative ΔG_f^0 values at 25 °C and 1 bar for some REE aqueous ions have been recommended later ([Gysi and Harlov, 2021](#); [Gysi et al., 2018](#); [Pan et al., 2024b](#)) ([Table 4](#)). In [Gysi and Harlov \(2021\)](#); [Gysi et al. \(2018\)](#), and [Pan et al. \(2024b\)](#), the ΔG_f^0 at 25 °C and 1 bar

for some REE aqueous ions were optimized by matching with the monazite and xenotime solubility experimental data at elevated temperatures (100–250 °C) without modifying the Helgeson-Kirkham-Flowers (HKF) parameters (Helgeson et al., 1981). In the low-temperature study of Pan et al. (2024b) the ΔG_f^0 at 25 °C and 1 bar were optimized based on the rhabdophane solubility data from Gausse et al. (2016) at the temperature range of 25–90 °C.

Here, we evaluated the ΔG_n^0 for aqueous REE³⁺ ions calculated from the alternative ΔG_f^0 and plotted them on the LFER relationships for the 16 isostructural families. The same ΔG_s^0 from Eqs. 2–5 and the same β parameters in Table 3 were used to calculate $\Delta G'_f$ and $\Delta G'_n$ values, respectively. Only experimental data used for the linear regression were plotted (Fig. 12). The REE₂O₃ C-Type and REE(OH)₃ isostructural mineral families were selected as examples (Fig. 12).

For REE₂O₃ C-Type, the LFER would not hold if the ΔG_f^0 of REE³⁺ ion recommended by Pan et al. (2024b) for high temperature experiments and by Gysi et al. (2018) and Gysi and Harlov (2021) are used. For, REE(OH)₃, the LFER would not hold if the ΔG_f^0 of REE³⁺ ion recommended by Pan et al. (2024a) for high-temperature experiments and by Gysi et al. (2018) and Gysi and Harlov (2021) are used, but those from Pan et al. (2024a) that were fitted from rhabdophane solubility data at the low temperature range of 25–90 °C would hold. As noted earlier, the “alternative” ΔG_f^0 at 25 °C and 1 bar for some REE aqueous ions were obtained by fitting solubility experimental data without adjusting the HKF parameters for temperature and pressure extrapolations. Solubility-derived ΔG_f^0 also depends on the HKF parameters. It is beyond the scope of the current study for a systematic evaluation of HKF parameters for the REE aqueous speciation model; This will be part of the future efforts.

6. Conclusions

Using the linear free energy relationship (LFER) recommended by Sverjensky and Molling (1992), we evaluated the internal consistency of the Gibbs free energy values for REE minerals and other crystalline solids in literature. We found remarkable linear correlations among $\Delta G_f^0 - \beta r$ values of the experimental values against ΔG_n^0 of REE ions within an isostructural family. The linear correlations also allowed us to identify the outliers and predict values for those end-members that are neither experimentally available nor appear to be outliers. Based on these evaluations, we recommend a set of standard Gibbs free energy of formation for

REE minerals and crystalline solids at 25 °C and 1 bar. For completeness, we included the heat capacity, entropy, and molar volumes from the literature to enable calculations to elevated temperatures and pressures (e.g., up to 1000 °C and 5 kb) (Table 5). These recommended thermodynamic properties have been incorporated into the SUPCRTBL program (Zimmer et al., 2016), which is available at models.earth.indiana.edu. These thermodynamic databases will also be incorporated into the MINES database to be used together with the GEMS code package in the future.

Data availability

All data generated for this study is included in the article.

CRedit authorship contribution statement

Ruiguang Pan: Investigation, Data curation, Formal analysis, Visualization, Writing original draft. **Chen Zhu:** Conceptualization, Methodology, Supervision, Visualization, Writing original draft, review and editing.

Declaration of competing interest

The authors declare that they have no known competing financial interests or personal relationships that could have appeared to influence the work reported in this paper.

Acknowledgments

This research is based upon work partially supported by the U.S. Department of Energy, Office of Science, Office of Basic Energy Sciences, Geosciences program under Award Number DE-SC0022269 to CZ.

References

- Atwood, D.A., 2013. The rare earth elements: fundamentals and applications. John Wiley & Sons.
- Baker, F.B., Fitzgibbon, G.C., Pavone, D., Holley Jr, C., Hansen, L.D., Lewis, E.A., 1972. Enthalpies of formation of Sm₂O₃ (monoclinic) and Sm₂O₃ (cubic). *The Journal of Chemical Thermodynamics* 4(4), 621-636.
- Baker, F.B., Holley, C.E., 1968. Enthalpy of formation of cerium sesquioxide. *Journal of Chemical & Engineering Data* 13(3), 405-407.
- Baloch, A.A., Alqahtani, S.M., Mumtaz, F., Muqaibel, A.H., Rashkeev, S.N., Alharbi, F.H., 2021. Extending Shannon's ionic radii database using machine learning. *Physical Review Materials* 5(4), 043804.
- Brookins, D.G., 1988. Eh-pH diagrams for geochemistry. Springer Science & Business Media.
- Chandrasekhar, M., Sunitha, D., Dhananjaya, N., Nagabhushana, H., Sharma, S., Nagabhushana, B., Shivakumara, C., Chakradhar, R., 2012. Structural and phase dependent thermo and photoluminescent properties of Dy (OH)₃ and Dy₂O₃ nanorods. *Materials Research Bulletin* 47(8), 2085-2094.
- Cordfunke, E., Konings, R., 2001. The enthalpies of formation of lanthanide compounds: III. Ln₂O₃ (cr). *Thermochimica Acta* 375(1-2), 65-79.
- Cotton, S., 2024. Lanthanide and actinide chemistry. John Wiley & Sons.
- Diakonov, I., Tagirov, B., Ragnarsdottir, K., 1998. Standard thermodynamic properties and heat capacity equations for rare earth element hydroxides: I. La (OH)₃ (s) and Nd (OH)₃ (s). Comparison of thermochemical and solubility data. *Radiochimica Acta* 81(2), 107-116.
- Eyring, L., Lohr, H., Cunningham, B., 1952. Heats of Reaction of Some Oxides of Americium and Praseodymium with Nitric Acid and an Estimate of the Potentials of the Am (III)—Am (IV) and Pr (III)—Pr (IV) Couples I. *Journal of the American Chemical Society* 74(5), 1186-1190.
- Fernández, D., Goodwin, A., Sengers, J.L., 1995. Measurements of the relative permittivity of liquid water at frequencies in the range of 0.1 to 10 kHz and at temperatures between 273.1 and 373.2 K at ambient pressure. *International journal of thermophysics* 16, 929-955.
- Fitzgibbon, G., EJ JR, H., CE JR, H., 1973. The enthalpies of formation of Pr₂O₃ (hexagonal), Pr₂O₃ (cubic), and PrO_{1.833}.
- Fitzgibbon, G.C., Holley Jr, C.E., Wadsö, I., 1965. The heat of formation of lanthanum oxide. *The Journal of Physical Chemistry* 69(7), 2464-2466.
- Fitzgibbon, G.C., Huber Jr, E.J., Holley Jr, C.E., 1972. Enthalpy of formation of europium sesquioxide. *The Journal of Chemical Thermodynamics* 4(3), 349-358.
- Fitzgibbon, G.C., Pavone, D., Holley, C.E., 1968. Enthalpy of formation of Nd₂O₃-hexagonal. *Journal of Chemical & Engineering Data* 13(4), 547-548.
- Gausse, C., Szenknect, S., Qin, D.W., Mesbah, A., Clavier, N., Neumeier, S., Bosbach, D.,

- Dacheux, N., 2016. Determination of the Solubility of Rhabdophanes $\text{LnPO}_4 \cdot 0.667\text{H}_2\text{O}$ (Ln = La to Dy). *European Journal of Inorganic Chemistry* 2016(28), 4615-4630. doi.org/10.1002/ejic.201600517.
- Gavrichev, K.S., Ryumin, M.A., Khoroshilov, A.V., Nikiforova, G.E., Tyurin, A.V., Gurevich, V.M., Starykh, R.V., 2013. Thermodynamic properties and phase transitions of tetragonal modification of terbium orthophosphate. *Vestnik (Herald) of St.Petersburg State University*.
- Gavrichev, K.S., Ryumin, M.A., Tyurin, A.V., Gurevich, V.M., Khoroshilov, A.V., Komissarova, L.N., 2012. Thermodynamic functions of erbium orthophosphate ErPO_4 in the temperature range of 0-1600 K. *Thermochimica Acta* 535, 1-7. doi.org/10.1016/j.tca.2012.02.002.
- Gavrichev, K.S., Ryumin, M.A., Tyurin, A.V., Gurevich, V.M., Komissarova, L.N., 2010. Heat Capacity and Thermodynamic Functions of Xenotime $\text{YPO}_4(\text{c})$ at 0-1600 K. *Geochemistry International* 48(9), 932-939. doi.org/10.1134/S0016702910090065.
- Gavrichev, K.S., Smirnova, N.N., Gurevich, V.M., Danilov, V.P., Tyurin, A.V., Ryumin, M.A., Komissarova, L.N., 2006. Heat capacity and thermodynamic functions of LuPO_4 in the range 0-320 K. *Thermochimica Acta* 448(1), 63-65. doi.org/10.1016/j.tca.2006.05.019.
- Goodenough, K.M., Wall, F., Merriman, D., 2018. The rare earth elements: demand, global resources, and challenges for resourcing future generations. *Natural Resources Research* 27, 201-216.
- Grandell, L., Lehtilä, A., Kivinen, M., Koljonen, T., Kihlman, S., Lauri, L.S., 2016. Role of critical metals in the future markets of clean energy technologies. *Renewable Energy* 95, 53-62.
- Gruber, J.B., Justice, B.H., Westrum Jr, E.F., Zandi, B., 2002. Revisiting the thermophysical properties of the A-type hexagonal lanthanide sesquioxides between temperatures of 5 K and 1000 K. *The Journal of Chemical Thermodynamics* 34(4), 457-473.
- Gvelesiani, G., Yashvili, T., 1967. Standard heats of formation of lanthanum and samarium sesquioxides. *Zhurnal Neorganicheskoi Khimii* 12(12), 3233-3236.
- Gysi, A.P., Harlov, D., 2021. Hydrothermal solubility of TbPO_4 , HoPO_4 , TmPO_4 , and LuPO_4 xenotime endmembers at pH of 2 and temperatures between 100 and 250 °C. *Chemical Geology* 567, 120072. doi.org/10.1016/j.chemgeo.2021.120072.
- Gysi, A.P., Harlov, D., Miron, G.D., 2018. The solubility of monazite (CePO_4), SmPO_4 , and GdPO_4 in aqueous solutions from 100 to 250 °C. *Geochimica et Cosmochimica Acta* 242, 143-164. doi.org/10.1016/j.gca.2018.08.038.
- Gysi, A.P., Williams-Jones, A.E., Harlov, D., 2015. The solubility of xenotime-(Y) and other HREE phosphates (DyPO_4 , ErPO_4 and YbPO_4) in aqueous solutions from 100 to 250 °C and p sat. *Chemical Geology* 401, 83-95. doi.org/10.1016/j.chemgeo.2015.02.023.
- Helean, K.B., Begg, B.D., Navrotsky, A., Ebbinghaus, B., Weber, W.J., Ewing, R., 2000. Enthalpies of formation of $\text{Gd}_2(\text{Ti}_{2-x}\text{Zr}_x)\text{O}_7$ pyrochlores. *MRS Online Proceedings Library (OPL)* 663, 691.

- Helgeson, H.C., Kirkham, D.H., Flowers, G.C., 1981. Theoretical prediction of the thermodynamic behavior of aqueous electrolytes by high pressures and temperatures; IV, Calculation of activity coefficients, osmotic coefficients, and apparent molal and standard and relative partial molal properties to 600 degrees C and 5kb. *American journal of science* 281(10), 1249-1516.
- Hennig, C., Oppermann, H., 1997. Thermal decomposition and solution calorimetry of ammonium samarium chlorides; Thermische Zersetzung und Lösungskalorimetrie von Ammoniumsamariumchloriden. *Zeitschrift fuer Naturforschung, B: Chemical Sciences* 52.
- Hennig, C., Oppermann, H., 1998. Thermische Zersetzung und Lösungskalorimetrie von Ammoniumneodymchloriden/Thermal Decomposition and Solution Calorimetry of Ammonium Neodymium Chlorides. *Zeitschrift für Naturforschung B* 53(2), 175-183.
- Huber Jr, E.J., Fitzgibbon, G.C., Holley Jr, C.E., 1964. The Heat of Formation of Europium Sesquioxide¹. *The Journal of Physical Chemistry* 68(9), 2720-2722.
- Huber Jr, E.J., Head, E.L., Holley Jr, C.E., 1956a. The heat of combustion of Erbium. *The Journal of Physical Chemistry* 60(11), 1582-1582.
- Huber Jr, E.J., Head, E.L., Holley Jr, C.E., 1956b. The heats of combustion of Dysprosium and Ytterbium. *The Journal of Physical Chemistry* 60(10), 1457-1458.
- Huber Jr, E.J., Head, E.L., Holley Jr, C.E., 1957. The heat of combustion of holmium. *The Journal of Physical Chemistry* 61(7), 1021-1022.
- Huber Jr, E.J., Holley Jr, C.E., 1952. The heat of combustion of neodymium. *Journal of the American Chemical Society* 74(21), 5530-5531.
- Huber Jr, E.J., Matthews, C.O., Holley Jr, C.E., 1955. The heat of combustion of samarium. *Journal of the American Chemical Society* 77(24), 6493-6494.
- Huntelaar, M., Booij, A., Cordfunke, E., Van der Laan, R., Van Genderen, A., Van Miltenburg, J., 2000. The thermodynamic properties of Ce₂O₃ (s) from T → 0 K to 1500 K. *The Journal of Chemical Thermodynamics* 32(4), 465-482.
- Igarashi, K., Mochinaga, J., 1987. Volume Changes on Melting for Several Rare Earth Chlorides. *Zeitschrift für Naturforschung A* 42(7), 777-778.
- Iloeje, C.O., Jové Colón, C.F., Cresko, J., Graziano, D.J., 2019. Gibbs energy minimization model for solvent extraction with application to rare-earths recovery. *Environmental Science & Technology* 53(13), 7736-7745.
- Johnson, G.K., Van Deventer, E.H., Kruger, O.L., Hubbard, W.N., 1969. The enthalpies of formation of plutonium dioxide and plutonium mononitride. *The Journal of Chemical Thermodynamics* 1(1), 89-98.
- Justice, B.H., Westrum Jr, E.F., 1963. Thermophysical properties of the lanthanide oxides. I. heat capacities, thermodynamic properties, and some energy levels of lanthanum (III) and neodymium (III) oxides from 5 to 350 °K. *The Journal of Physical Chemistry* 67(2), 339-345.
- Justice, B.H., Westrum Jr, E.F., 1969. Thermophysical properties of the lanthanide oxides. V.

- Heat capacity, thermodynamic properties, and energy levels of cerium (III) oxide. *The Journal of Physical Chemistry* 73(6), 1959-1962.
- Karapet'yants, M.K., Maier, A., Bas' kova, N., 1977. Gibbs standard energies of formation of rare-earth and yttrium carbonates and their entropies. *Izv. Akad. Nauk SSSR, Neorg. Mater.:(USSR)* 13(6).
- Konings, R., Kovács, A., 2003. Thermodynamic properties of the lanthanide (III) halides. *Handbook on the physics and chemistry of rare earths* 33, 147-247.
- Konings, R.J., Beneš, O., 2010. The thermodynamic properties of the f-elements and their compounds. I. The lanthanide and actinide metals. *Journal of Physical and Chemical Reference Data* 39(4).
- Konings, R.J.M., Beneš, O., Kovács, A., Manara, D., Sedmidubský, D., Gorokhov, L., Iorish, V.S., Yungman, V., Shenyavskaya, E., Osina, E., 2014. The Thermodynamic Properties of the f-Elements and their Compounds: Part 2. The Lanthanide and Actinide Oxides. *Journal of Physical and Chemical Reference Data* 43(1). doi.org/10.1063/1.4825256.
- Kuznetsov, F., Rezhukhina, T., Golubenko, A., 1960. Determination of the heat of formation of Cerium (III) oxide by combustion in a bomb calorimeter. *Russian Journal of Physical Chemistry* 34(9), 1010-1010.
- Lemire, R.J., 2001. Chemical thermodynamics of neptunium and plutonium.
- Liu, X., Byrne, R.H., 1997. Rare earth and yttrium phosphate solubilities in aqueous solution. *Geochimica et Cosmochimica Acta* 61(8), 1625-1633. doi.org/10.1016/S0016-7037(97)00037-9.
- Mah, A.D., 1961. Heats of Formation of Cerium Sesquioxide and Bismuth Sesquioxide by Combustion Calorimetry. US Department of the Interior, Bureau of Mines.
- Martell, A.E., Smith, R.M., 1974. Critical stability constants: Inorganic complexes.-1976.- (RUI dnr.: M103585287). Plenum Press.
- Migdisov, A., Guo, X., Nisbet, H., Xu, H., Williams-Jones, A.E., 2019. Fractionation of REE, U, and Th in natural ore-forming hydrothermal systems: Thermodynamic modeling. *Journal of Chemical Thermodynamics* 128, 305-319. doi.org/10.1016/j.jct.2018.08.032.
- Migdisov, A., Williams-Jones, A.E., Brugger, J., Caporuscio, F.A., 2016. Hydrothermal transport, deposition, and fractionation of the REE: Experimental data and thermodynamic calculations. *Chemical Geology* 439, 13-42. doi.org/10.1016/j.chemgeo.2016.06.005.
- Migdisov, A.A., Williams-Jones, A.E., Wagner, T., 2009. An experimental study of the solubility and speciation of the Rare Earth Elements (III) in fluoride- and chloride-bearing aqueous solutions at temperatures up to 300 °C. *Geochimica et Cosmochimica Acta* 73(23), 7087-7109. doi.org/10.1016/j.gca.2009.08.023.
- Montgomery, R.L., Hubert, T.D., 1959. Thermochemistry of samarium. US Department of the Interior, Bureau of Mines.
- Morss, L., Fuger, J., 1981. Enthalpy formation of americium dioxide and a thermochemical estimate of the electrode potential Am^{4+}/Am^{3+} . *Journal of Inorganic and Nuclear Chemistry* 43(9), 2059-2064.

- Morss, L., Konings, R., 2004. Thermochemistry of binary rare earth oxides, Binary Rare Earth Oxides. Springer, pp. 163-188.
- Morss, L.R., Day, P.P., Felinto, C., Brito, H., 1993. Standard molar enthalpies of formation of Y₂O₃, Ho₂O₃, and Er₂O₃ at the temperature 298.15 K. The Journal of Chemical Thermodynamics 25(3), 415-422.
- Morss, L.R., Haar, C.M., Mroczkowski, S., 1989. Standard molar enthalpy of formation of neodymium hydroxide. The Journal of Chemical Thermodynamics 21(10), 1079-1083.
- Mroczkowski, S., Eckert, J., Meissner, H., Doran, J., 1970. Hydrothermal growth of single crystals of rare earth hydroxides. Journal of Crystal Growth 7(3), 333-342.
- Navrotsky, A., Lee, W., Mielewczyk-Gryn, A., Ushakov, S.V., Anderko, A., Wu, H., Riman, R.E., 2015. Thermodynamics of solid phases containing rare earth oxides. Journal of Chemical Thermodynamics 88, 126-141. doi.org/10.1016/j.jct.2015.04.008.
- Ni, Y., Hughes, J.M., Mariano, A.N., 1995. Crystal chemistry of the monazite and xenotime structures. American Mineralogist 80(1-2), 21-26. doi.org/10.2138/am-1995-1-203.
- OECD, 1985. The organisation for economic co-operation and development. OEEC Paris, France.
- Oppermann, H., Morgenstern, A., Ehrlich, S., 1997. Calorimetrie an Lanthantrihalogeniden und Ammoniumlanthanhalogeniden/Calorimetry of Lanthanum Trihalides and of Ammonium Lanthanum Halides. Zeitschrift für Naturforschung B 52(9), 1062-1066.
- Pan, R., Gysi, A.P., Migdisov, A., Gong, L., Lu, P., Zhu, C., 2024a. Linear correlations of Gibbs free energy of REE phosphates (monazite, xenotime, and rhabdophane) and internally consistent binary mixing properties. Minerals 14(3). doi.org/10.3390/min14030305.
- Pan, R., Gysi, A.P., Miron, G.D., Zhu, C., 2024b. Optimized thermodynamic properties of REE aqueous species (REE³⁺ and REE(OH)₂⁺) and experimental database for modeling the solubility of REE phosphate minerals (monazite, xenotime, and rhabdophane) from 25 to 300 °C. Chemical Geology 643, 121817. doi.org/10.1016/j.chemgeo.2023.121817.
- Pankratz, L., 1984. Thermodynamic properties of halides. United States Department of the Interior, Bureau of Mines.
- Popova, A., Monaenkova, A., 1989. Standard formation enthalpy of neodymium oxide of hexagonal structure. Zhurnal Fizicheskoy Khimii 63(9), 2340-2343.
- Putnam, R.L., Navrotsky, A., Cordfunke, E., Huntelaar, M., 2000. Thermodynamics of formation of two cerium aluminum oxides, CeAlO₃ (s) and CeAl₁₂O₁₉. 918 (s), and cerium sesquioxide, Ce₂O₃ (s) at T= 298.15 K. The Journal of Chemical Thermodynamics 32(7), 911-921.
- Ragavan, A.J., Adams, D.V., 2009. Estimation of equilibrium surface precipitation constants for trivalent metal sorption onto hydrous ferric oxide and calcite. Journal of Nuclear Materials 389(3), 394-401.
- Robie, R.A., Hemingway, B.S., Fisher, J.R., 1978. Thermodynamic properties of minerals and related substances at 298. 15 k and 1 bar (10⁵/sup 5/pascals) pressure and at higher temperatures. Geological Survey, Washington, DC (USA).

- Rossini, F.D., 1961. Selected values of chemical thermodynamic properties: references. US Government Printing Office.
- Schumm, R., Wagman, D.D., Bailey, S., Evans, W., Parker, V.B., 1973. Selected values of chemical thermodynamic properties: tables for the lanthanide (rare earth) elements (elements 62 through 76 in the standard order of arrangement). US Government Printing Office.
- Shannon, R.D., 1976. Revised effective ionic radii and systematic studies of interatomic distances in halides and chalcogenides. *Acta crystallographica section A: crystal physics, diffraction, theoretical and general crystallography* 32(5), 751-767.
- Shannon, R.T., Prewitt, C.T., 1969. Effective ionic radii in oxides and fluorides. *Acta Crystallographica Section B: Structural Crystallography and Crystal Chemistry* 25(5), 925-946.
- Shock, E.L., Helgeson, H.C., 1988. Calculation of the thermodynamic and transport properties of aqueous species at high pressures and temperatures: Correlation algorithms for ionic species and equation of state predictions to 5 kb and 1000°C. *Geochimica et Cosmochimica Acta* 52(8), 2009-2036. doi.org/10.1016/0016-7037(88)90181-0.
- Shock, E.L., Sassani, D.C., Willis, M., Sverjensky, D.A., 1997. Inorganic species in geologic fluids: Correlations among standard molal thermodynamic properties of aqueous ions and hydroxide complexes. *Geochimica et Cosmochimica Acta* 61(5), 907-950. doi.org/10.1016/S0016-7037(96)00339-0.
- Silva, R.J., Bidoglio, G., Robouch, P., Puigdomenech, I., Wanner, H., Rand, M., 2012. Chemical thermodynamics of americium. Newnes.
- Spedding, F., Miller, C.F., 1952. Thermochemistry of the rare earths. I. Cerium and neodymium. *Journal of the American Chemical Society* 74(16), 4195-4198.
- Spedding, F.H.E., R.E. Naumann, A.W. , 1959. Technical Report ISC-934. US Atomic Energy Community.
- Stokłosa, A., 2012. Molar Volume, Ionic Radii in Stoichiometric and Nonstoichiometric Metal Oxides. *Stoichiometry and Materials Science: When Numbers Matter*, 219.
- Stubblefield, C., Eick, H., Eyring, L., 1956. Terbium oxides. II. The heats of formation of several oxides. *Journal of the American Chemical Society* 78(16), 3877-3879.
- Stuve, J.M., 1965. Heat of formation of europium sesquioxide and europium trichloride. US Department of the Interior, Bureau of Mines.
- Sverjensky, D.A., Molling, P., 1992. A linear free energy relationship for crystalline solids and aqueous ions. *Nature* 356(6366), 231-234.
- Thoenen, T., Hummel, W., Berner, U., Curti, E., 2014. The PSI/Nagra Chemical Thermodynamic Database 12/07.
- Wang, Y., Xu, H., 1999. Thermodynamic stability of actinide pyrochlore minerals in deep geologic repository environments. *MRS Online Proceedings Library (OPL)* 608.
- Wang, Y., Xu, H., 2001. Prediction of trace metal partitioning between minerals and aqueous solutions: a linear free energy correlation approach. *Geochimica et Cosmochimica Acta*

- 65(10), 1529-1543.
- Xu, H., Wang, Y., 1999a. Use of linear free energy relationship to predict Gibbs free energies of formation of MUO_4 phases. *Radiochimica Acta* 87(1-2), 37-40.
- Xu, H., Wang, Y., 1999b. Use of linear free energy relationship to predict Gibbs free energies of formation of pyrochlore phases (CaMTi_2O_7). *Journal of Nuclear Materials* 275(2), 216-220.
- Xu, H., Wang, Y., 1999c. Use of linear free energy relationship to predict Gibbs free energies of formation of zirconolite phases (MZrTi_2O_7 and MHfTi_2O_7). *Journal of Nuclear Materials* 275(2), 211-215.
- Zhang, B., Liu, C., Li, C., Jiang, M., 2016. Separation and recovery of valuable metals from low-grade REE–Nb–Fe ore. *International Journal of Mineral Processing* 150, 16-23.
- Zhu, C., 2002. Estimation of surface precipitation constants for sorption of divalent metals onto hydrous ferric oxide and calcite. *Chemical Geology* 188(1-2), 23-32.
- Zimmer, K., Zhang, Y., Lu, P., Chen, Y., Zhang, G., Dalkilic, M., Zhu, C., 2016. SUPCRTBL: A revised and extended thermodynamic dataset and software package of SUPCRT92. *Computers and Geosciences* 90, 97-111. doi.org/10.1016/j.cageo.2016.02.013.
- Zinkevich, M., 2007. Thermodynamics of rare earth sesquioxides. *Progress in Materials Science* 52(4), 597-647. doi.org/10.1016/j.pmatsci.2006.09.002.

Tables

Table 1. List of symbols and definitions

Symbol	Definition
ΔG_f°	Gibbs free energy of formation
ΔG_n°	Non-solvation contribution to the Gibbs energy of formation
ΔG_s°	Solvation contribution to the Gibbs energy of formation
$\Delta G'_f$	Adjusted Gibbs free energy of formation ($\Delta G_{f, \text{REEX}}^{\circ} - \beta r_{\text{REE}^{Z+}}$)
ΔS_f°	Entropy of formation from the elements
S°	Standard entropy
ΔH_f°	Enthalpy of formation from the elements
C_p	Heat capacity
V°	Molar volume
R	Gas constant ($8.314 \text{ J mol}^{-1} \text{ K}^{-1}$)
K	Equilibrium products
K_{sp}	Solubility constants
ω	Born coefficient of an ion
ω^{abs}	Absolute Born coefficient of an ion
$r_{\text{REE}^{Z+}}$	Crystallographic radius of the aqueous REE^{Z+} ion
Z	Charge number of an ion
MX	Chemical formula of a solid
REE	Rare Earth Elements

Table 2. Ionic radii and thermodynamic data for REE cations and minerals

REE Ions	¹ C.N.	r(REE ³⁺)	ΔG_s° (kJ mol ⁻¹)	ΔG_f° (kJ mol ⁻¹)	ΔG_n° (kJ mol ⁻¹)	V° (cm ³ mol ⁻¹)	ΔG_f° (kJ mol ⁻¹)	Crystal Structure
		Å	REE ³⁺ _(aq)	REE ³⁺ _(aq)	REE ³⁺ _(aq)	² REE ₂ O _{3(s)}	³ REE ₂ O _{3(s)}	
La	7	1.100	-906.99	-686.18	220.82	49.63	-1704.06	A-Type
Ce	7	1.070	-919.13	-676.13	243.00	47.84	-1710.65	A-Type
Pr	7	⁴ 1.056	-924.82	-680.32	244.51	46.68	-1719.71	A-Type
Nd	7	⁴ 1.043	-930.43	-671.95	258.48	45.89	-1719.30	A-Type
Pm	6	0.970	-961.00	-665.68	295.33	45.70	-1724.02	B-Type
Sm	6	0.958	-966.17	-665.67	300.50	45.08	-1734.65	B-Type
Eu	6	0.947	-970.94	-574.46	396.48	44.25	-1553.58	B-Type
Gd	6	0.938	-974.87	-663.58	311.29	43.40	-1734.21	B-Type
Cm	6	0.970	-961.00	⁵ -595.40	365.60	-	-1599.82	B-Type
Eu	6	0.947	-970.94	-574.46	396.48	48.33	-1564.72	C-Type
Gd	6	0.938	-974.87	-663.58	311.29	47.57	-1766.57	C-Type
Tb	6	0.923	-981.45	-667.35	314.10	46.47	-1777.84	C-Type
Dy	6	0.912	-986.31	-664.00	322.31	45.65	-1769.92	C-Type
Ho	6	0.901	-991.20	-675.30	315.90	44.91	-1793.34	C-Type
Er	6	0.890	-996.12	-669.02	327.10	44.16	-1809.57	C-Type
Tm	6	0.880	-1000.61	-669.02	331.59	43.41	-1795.52	C-Type
Yb	6	0.868	-1006.04	-640.15	365.89	42.76	-1726.73	C-Type
Lu	6	0.861	-1009.22	-666.93	342.29	42.23	-1792.65	C-Type
Y	6	0.900	-991.65	-685.34	306.31	44.80	-1844.06	C-Type
		Å	REE ⁴⁺ _(aq)	REE ⁴⁺ _(aq)	REE ⁴⁺ _(aq)	⁶ REEO _{2(s)}	³ REEO _{2(s)}	
Ce	8	0.970	-1429.77	-507.52	922.25	23.85	-1027.03	Cubic
Pr	8	0.960	-1434.68	-304.18	1130.50	23.61	-900.04	Cubic
Tb	8	0.880	-1474.76	-369.03	1105.73	21.41	-915.41	Cubic
Th	8	1.050	-1391.18	-704.78	686.40	26.40	-1169.24	Cubic
U	8	1.000	-1415.15	-529.90	885.25	24.64	-1031.83	Cubic
Np	8	0.980	-1424.87	⁷ -491.80	933.07	24.14	-1026.23	Cubic
Pu	8	0.960	-1434.68	⁷ -478.00	956.68	23.65	-998.11	Cubic
Am	8	0.950	-1439.62	⁸ -346.00	1093.62	23.37	-877.03	Cubic
		Å	REE ³⁺ _(aq)	REE ³⁺ _(aq)	REE ³⁺ _(aq)	REE(OH) _{3(s)}	¹¹ REE(OH) _{3(s)}	
La	9	1.216	-861.74	-686.18	175.56	⁹ 42.79	-1284.20	Cubic
Ce	9	1.196	-869.35	-676.13	193.22	-	-1286.40	Cubic

Pr	9	1.179	-875.89	-680.32	195.57	⁹ 40.64	-1284.90	Cubic
Nd	9	1.163	-882.09	-671.95	210.14	⁹ 39.44	-1283.00	Cubic
Pm	9	1.144	-889.51	-665.68	223.84	-	-	Cubic
Sm	9	1.132	-894.24	-665.67	228.57	⁹ 38.38	-1273.30	Cubic
Eu	9	1.120	-899.00	-574.46	324.54	⁹ 37.81	-1180.60	Cubic
Gd	9	1.107	-904.19	-663.58	240.60	⁹ 37.36	-1276.20	Cubic
Tb	9	1.095	-909.00	-667.35	241.65	⁹ 36.49	-1281.10	Cubic
Dy	9	1.083	-913.85	-664.00	249.85	¹⁰ 37.98	-1294.80	Cubic
Ho	9	1.072	-918.32	-675.30	243.02	⁹ 35.84	-1297.40	Cubic
Er	9	1.062	-922.40	-669.02	253.38	-	-1298.90	Cubic
Tm	9	1.052	-926.51	-669.02	257.49	-	-1286.60	Cubic
Yb	9	1.042	-930.64	-640.15	290.49	-	-1262.90	Cubic
Lu	9	1.032	-934.79	-666.93	267.86	-	-	Cubic
Y	9	1.075	-917.10	-685.34	231.76	35.96	-1338.50	Cubic
		Å	REE ³⁺ _(aq)	REE ³⁺ _(aq)	REE ³⁺ _(aq)	¹² REECl _{3(s)}	¹³ REECl _{3(s)}	
La	9	1.216	-861.74	-686.18	175.56	63.90	-995.89	UCl ₃
Ce	9	1.196	-869.35	-676.13	193.22	-	-983.61	UCl ₃
Pr	9	1.179	-875.89	-680.32	195.57	61.40	-982.72	UCl ₃
Nd	9	1.163	-882.09	-671.95	210.14	60.47	-965.56	UCl ₃
Sm	9	1.132	-894.24	-665.67	228.57	-	-949.55	UCl ₃
Eu	9	1.120	-899.00	-574.46	324.54	-	-855.39	UCl ₃
Gd	9	1.107	-904.19	-663.58	240.60	58.03	-943.28	UCl ₃
Tb	8	0.923	-981.45	-667.35	314.10	-	-	PuBr ₃
Dy	6	0.912	-986.31	-664.00	322.31	74.38	-923.34	AlCl ₃
Ho	6	0.901	-991.20	-675.30	315.90	-	-928.29	AlCl ₃
Er	6	0.890	-996.12	-669.02	327.10	-	-925.02	AlCl ₃
Tm	6	0.880	-1000.61	-669.02	331.59	-	-926.20	AlCl ₃
Yb	6	0.868	-1006.04	-640.15	365.89	-	-892.36	AlCl ₃
Lu	6	0.861	-1009.22	-666.93	342.29	-	-917.76	AlCl ₃
Y	6	0.900	-991.65	-685.34	306.31	74.83	-	AlCl ₃
		Å	REE ³⁺ _(aq)	REE ³⁺ _(aq)	REE ³⁺ _(aq)	¹⁴ REEF _{3(s)}	¹⁵ REEF _{3(s)}	
La	9	1.216	-861.74	-686.18	175.56	33.00	-1649.81	LaF ₃
Ce	9	1.196	-869.35	-676.13	193.22	32.01	-1641.37	LaF ₃
Pr	9	1.179	-875.89	-680.32	195.57	31.53	-1641.37	LaF ₃

Nd	9	1.163	-882.09	-671.95	210.14	30.93	-1634.37	LaF ₃
Sm	9	1.132	-894.24	-665.67	228.57	31.24	-1625.67	YF ₃
Eu	9	1.120	-899.00	-574.46	324.54	30.76	-	YF ₃
Gd	9	1.107	-904.19	-663.58	240.60	30.36	-1619.60	YF ₃
Tb	9	1.095	-909.00	-667.35	241.65	29.87	-1620.78	YF ₃
Dy	9	1.083	-913.85	-664.00	249.85	29.40	-1615.77	YF ₃
Ho	9	1.072	-918.32	-675.30	243.02	29.02	-1623.61	YF ₃
Er	9	1.062	-922.40	-669.02	253.38	28.68	-1616.38	YF ₃
Tm	9	1.052	-926.51	-669.02	257.49	28.40	-1614.56	YF ₃
Yb	9	1.042	-930.64	-640.15	290.49	28.16	-1587.69	YF ₃
Lu	9	1.032	-934.79	-666.93	267.86	27.97	-1609.06	YF ₃
Y	9	1.075	-917.10	-685.34	231.76	-	-	YF ₃
		Å	REE ³⁺ _(aq)	REE ³⁺ _(aq)	REE ³⁺ _(aq)	REE ₂ (CO ₃) _{3(s)}	REE ₂ (CO ₃) _{3(s)}	
La	6	1.032	-934.79	-686.18	248.61	-	¹¹ -3141.77	-
Ce	6	1.010	-943.99	-676.13	267.86	-	-	-
Pr	6	0.990	-952.45	-680.32	272.13	-	-	-
Nd	6	0.983	-955.43	-671.95	283.48	-	¹¹ -3102.02	-
Pm	6	0.970	-961.00	-665.68	295.33	-	-	-
Sm	6	0.958	-966.17	-665.67	300.50	-	¹¹ -3102.02	-
Eu	6	0.947	-970.94	-574.46	396.48	-	-	-
Gd	6	0.938	-974.87	-663.58	311.29	-	-	-
Tb	6	0.923	-981.45	-667.35	314.10	-	-	-
Dy	6	0.912	-986.31	-664.00	322.31	-	¹⁶ -3093.23	-
Ho	6	0.901	-991.20	-675.30	315.90	-	-	-
Er	6	0.890	-996.12	-669.02	327.10	-	-	-
Tm	6	0.880	-1000.61	-669.02	331.59	-	-	-
Yb	6	0.868	-1006.04	-640.15	365.89	-	¹⁶ -3050.55	-
Lu	6	0.861	-1009.22	-666.93	342.29	-	-	-
Y	6	0.900	-991.65	-685.34	306.31	-	¹⁶ -3148.04	-
Am	6	0.975	-958854	⁸ -598.70	360.16	-	¹⁷ -2996.20	-
Pu	6	1.000	-948210	⁷ -512.87	369.23	-	¹⁷ -2918.09	-
		Å	REE ³⁺ _(aq)	REE ³⁺ _(aq)	REE ³⁺ _(aq)	REE ₂ (CO ₃) _{3.nH₂O(s)}	¹⁸ REE ₂ (CO ₃) _{3.nH₂O(s)}	
La	6	1.032	-934.79	-686.18	248.61	-	-4958.88	-
Ce	6	1.010	-943.99	-676.13	267.86	-	-4958.04	-

Pr	6	0.990	-952.45	-680.32	272.13	-	-4947.16	-
Nd	6	0.983	-955.43	-671.95	283.48	-	-4931.26	-
Pm	6	0.970	-961.00	-665.68	295.33	-	-	-
Sm	6	0.958	-966.17	-665.67	300.50	-	-3739.24	-
Eu	6	0.947	-970.94	-574.46	396.48	-	-3553.89	-
Gd	6	0.938	-974.87	-663.58	311.29	-	-3728.78	-
Tb	6	0.923	-981.45	-667.35	314.10	-	-3706.19	-
Dy	6	0.912	-986.31	-664.00	322.31	-	-3732.13	-
Ho	6	0.901	-991.20	-675.30	315.90	-	-3748.03	-
Er	6	0.890	-996.12	-669.02	327.10	-	-3736.31	-
Tm	6	0.880	-1000.61	-669.02	331.59	-	-3719.58	-
Y	6	0.900	-991.65	-685.34	306.31	-	-3783.59	-
		Å	REE ³⁺ _(aq)	REE ³⁺ _(aq)	REE ³⁺ _(aq)	REEFeO _{3(s)}	¹¹ REEFeO _{3(s)}	
La	12	1.360	-809.05	-686.18	122.88	-	-1277.80	Perovskite
Pr	12	⁴ 1.304	-829.00	-680.32	148.68	-	-1282.00	Perovskite
Nd	12	1.270	-841.55	-671.95	169.60	-	-1277.40	Perovskite
Sm	12	1.240	-852.70	-665.67	187.02	-	-1284.10	Perovskite
Eu	12	⁴ 1.224	-858.79	-574.46	284.32	-	-1194.50	Perovskite
Gd	12	⁴ 1.212	-863.37	-663.58	199.79	-	-1269.80	Perovskite
Tb	12	⁴ 1.201	-867.40	-667.35	200.06	-	-	Perovskite
Dy	12	⁴ 1.192	-871.00	-664.00	207.00	-	-1285.30	Perovskite
Ho	12	⁴ 1.183	-874.23	-675.30	198.93	-	-1289.10	Perovskite
Er	12	-	-	-669.02	-	-	-1287.80	Perovskite
Tm	12	⁴ 1.168	-880.11	-669.02	211.08	-	-	Perovskite
Yb	12	⁴ 1.161	-882.83	-640.15	242.67	-	-	Perovskite
Lu	12	-	-	-666.93	-	-	-	Perovskite
		Å	REE ³⁺ _(aq)	REE ³⁺ _(aq)	REE ³⁺ _(aq)	REE ₂ Zr ₂ O _{7(s)}	REE ₂ Zr ₂ O _{7(s)}	
La	8	1.160	-883.25	-686.18	197.08	-	¹¹ -3930.40	Pyrochlore
Ce	8	1.143	-889.91	-676.13	213.77	-	¹¹ -3923.20	Pyrochlore
Sm	8	1.079	-915.47	-665.67	249.80	-	¹¹ -3916.70	Pyrochlore
Gd	8	1.053	-926.10	-663.58	262.52	-	¹⁹ -3873.50	Pyrochlore

¹C.N.: Coordination number.

²Zinkevich (2007); ³Konings et al. (2014); ⁴Baloch et al. (2021); ⁵Thoenen et al. (2014); ⁶Morss and Fuger (1981); ⁷Lemire (2001); ⁸Silva et al. (2012); ⁹Mroczkowski et al. (1970); ¹⁰Chandrasekhar et al. (2012); ¹¹Navrotsky et al. (2015); ¹²Igarashi and Mochinaga (1987); ¹³Konings and

Kovács (2003); ¹⁴Migdisov et al. (2009); ¹⁵Migdisov et al. (2016); ¹⁶Martell and Smith (1974); ¹⁷OECD (1985); ¹⁸Karapet'yants et al. (1977); ¹⁹Helean et al. (2000). Note that references of other thermodynamic data can be found in Section 3.2.

Table 3. Summary of regression parameters for linear free energy correlation.

REEX	Structure	a	Parameters b (kJ mol ⁻¹)	β (kJ Å ⁻¹)	R ²
REE ₂ O ₃	A-Type	0.742 (-)	-2674.67 (-)	732.39 (-)	0.9995
REE ₂ O ₃	B-Type	2.043 (-)	-3056.77 (-)	732.04 (-)	0.9991
REE ₂ O ₃	C-Type	2.260 (0.178)	-3647.73 (160.52)	1258.34 (120.38)	0.9970
REEO ₂	Cubic	0.604 (0.057)	-1599.64 (207.16)	19.39 (163.56)	0.9930
REE(OH) ₃	Cubic	1.070 (0.040)	-2122.19 (42.27)	530.11(31.50)	0.9944
REECl ₃	UCl ₃	1.013 (0.031)	-1268.09 (54.64)	75.10 (42.84)	0.9985
REECl ₃	AlCl ₃	1.017 (0.147)	-1603.73 (193.47)	390.19 (171.97)	0.9830
REEF ₃	LaF ₃	0.566 (-)	-1844.46 (-)	78.29 (-)	0.9750
REEF ₃	YF ₃	0.867 (0.068)	-2021.58 (62.10)	174.66 (44.19)	0.9909
REE ₂ (CO ₃) ₃	-	2.098 (0.0789)	-4640.35 (51.24)	948.39 (49.84)	0.9988
REE ₂ (CO ₃) ₃ ·8H ₂ O	-	1.227 (-)	-5002.35 (-)	-281.58 (-)	0.9935
REE ₂ (CO ₃) ₃ ·3H ₂ O	-	2.0416 (0.114)	-4946.65 (109.66)	616.03 (134.88)	1.0000
REEFeO ₃	Perovskite	0.915 (0.070)	-2005.97 (93.38)	450.20 (69.11)	0.9878

Uncertainties of 2σ are given in parentheses for each regression parameter; Some parameters have no uncertainties because of that only 4 samples are available for the regression; All values refer to 25 °C and 1 bar.

Table 4. Thermodynamic data of ΔG_f^o (kJ mol⁻¹) for REE³⁺ ion from different sources

REE ³⁺	Shock et al. (1997)	Pan et al. (2024) High <i>T</i>	Diff.	Pan et al. (2024) Low <i>T</i>	Diff.	Gysi et al. (2018)	Diff.	Gysi and Harlov (2021)	Diff.
La	-686.18	-683.28	2.90	-684.58	1.60				
Ce	-676.13	-674.72	1.41	-674.11	2.02	-673.06	3.07		
Pr	-680.32	-682.14	-1.82	-679.24	1.08				
Nd	-671.95	-681.77	-9.82	-670.11	1.84				
Sm	-665.67	-669.33	-3.66	-664.12	1.55	-669.94	-4.27		
Eu	-574.46	-578.86	-4.40	-568.06	6.40				
Gd	-663.58	-672.41	-8.83	-662.07	1.51	-672.52	-8.93		
Tb	-667.35	-687.54	-20.19					-684.09	-16.74
Dy	-664.00	-686.85	-22.85						
Y	-685.34	-706.60	-21.26						
Ho	-675.30	-682.67	-7.37					-683.66	-8.36
Er	-669.02	-695.21	-26.19						
Tm	-669.02	-677.78	-8.76					-672.49	-3.47
Yb	-640.15	-642.97	-2.82						
Lu	-666.93	-665.54	1.39					-665.40	1.53

Table 5. Recommended standard thermodynamic properties of REE minerals at temperature of 298.15 K and pressure of 1 bar, and selected heat capacity function, with T in Kelvin. Fonts in red represent predicted values.

REEX	Crystal Structure	ΔG_f°	ΔH_f°	S°	V°	$C_p = a + bT + c/T^2 + d/T^{0.5}$				Temperature range	
		kJ mol ⁻¹	kJ mol ⁻¹	J K ⁻¹ mol ⁻¹	cm ³ mol ⁻¹	a	$b*100$	c	d	K	References
La ₂ O ₃	A-Type	-1704.06	-1791.60	127.32	49.63	120.6805	1.342414	-1413668	-	298–1800	K14
Ce ₂ O ₃	A-Type	-1710.65	-1799.80	148.10	47.84	113.736	2.84344	-641205	-	298–2392	K14
Pr ₂ O ₃	A-Type	-1719.71	-1809.90	152.70	46.68	121.6594	2.55611	-989420	-	298–2310	K14
Nd ₂ O ₃	A-Type	-1719.30	-1806.90	158.70	45.89	117.1079	2.813655	-1258450	-	298–2379	K14
Pm ₂ O ₃	A-Type	-	-	-	44.87	129.454	1.996	-	-	2013–2407	K14
Pm ₂ O ₃	B-Type	-1737.64	-1824.61	158.00	45.70	122.9493	3.00141	-1852170	-	298–2013	K14
Sm ₂ O ₃	B-Type	-1734.65	-1823.00	150.60	45.08	129.7953	1.903114	-1862270	-	298–2190	K14
Eu ₂ O ₃	B-Type	-1553.58	-1650.40	138.60	44.25	133.3906	1.66443	-1424350	-	298–2327	K14
Gd ₂ O ₃	B-Type	-1734.21	-1819.70	157.10	43.40	114.6104	1.52344	-1249170	-	298–2430	K14
Cm ₂ O ₃	B-Type	-1599.82	-1684.00	167.00	45.98	123.532	0.1455	-1348900	-	298–1888	K14
Pm ₂ O ₃	C-Type	-1759.73	-	-	49.96	-	-	-	-	-	K14
Sm ₂ O ₃	C-Type	-1763.14	-1826.80	233.42	49.20	132.4358	1.87799	-2408600	-	298–900	K14
Eu ₂ O ₃	C-Type	-1564.72	-1662.50	135.40	48.33	136.2978	1.49877	-1499300	-	298–1350	K14
Gd ₂ O ₃	C-Type	-1766.57	-1854.00	150.60	47.57	114.8086	1.72911	-1283970	-	298–2000	K14
Cm ₂ O ₃	C-Type	-1600.92	-	-	50.21	-	-	-	-	-	K14
Tb ₂ O ₃	C-Type	-1777.84	-1865.20	159.20	46.47	120.6682	2.217194	-1002610	-	298–1823	K14
Dy ₂ O ₃	C-Type	-1769.92	-1863.40	149.80	45.65	121.2302	1.527609	-845800	-	298–2223	K14
Ho ₂ O ₃	C-Type	-1793.34	-1883.30	156.38	44.91	121.934	1.011623	-886280	-	298–2538	K14
Er ₂ O ₃	C-Type	-1788.61	-1879.13	153.13	44.16	123.2921	0.862245	-1544330	-	298–2538	K14
Tm ₂ O ₃	C-Type	-1795.52	-1889.30	139.70	43.41	128.4322	0.523209	-1178910	-	298–2588	K14
Yb ₂ O ₃	C-Type	-1726.73	-1814.50	133.10	42.76	130.6438	0.334628	-1448200	-	298–2687	K14
Lu ₂ O ₃	C-Type	-1792.65	-1877.00	126.79	42.23	122.4593	0.729001	-2034140	-	298–2762	K14
Y ₂ O ₃	C-Type	-1823.00	-1911.74	98.96	44.80	122.91	0.743	-1931300	-	298–2000	MK05
CeO ₂	Cubic	-1027.03	-1090.40	62.29	23.85	74.4814	0.583682	-1297100	-	298–3083	K14
PrO ₂	Cubic	-900.04	-959.10	80.80	23.61	72.9881	1.6628	-99900	-	298–663	K14
TbO ₂	Cubic	-915.41	-972.20	86.90	21.41	73.259	1.32023	1042400	-	298–1400	K14

La(OH) ₃	Cubic	-1284.20	-1416.10	117.80	42.79	521.7845	-40.255	709538.23	-5081.56	200–350	D98
Ce(OH) ₃	Cubic	-1286.40	-1418.60	129.40	41.47	-	-	-	-	-	-
Pr(OH) ₃	Cubic	-1284.90	-1404.00	131.70	40.64	520.9956	-40.327	771992.59	-5070.02	10–350	D98
Nd(OH) ₃	Cubic	-1283.00	-1415.60	129.90	39.44	254.8777	-2.25	366050.62	-2324.81	10–350	D98
Pm(OH) ₃	Cubic	-1276.30	-	-	38.97	-	-	-	-	-	-
Sm(OH) ₃	Cubic	-1273.30	-1406.60	125.80	38.38	-	-	-	-	-	-
Eu(OH) ₃	Cubic	-1180.60	-1319.10	119.90	37.81	518.63	-38.286	705759.72	-5035.37	200–350	D98
Gd(OH) ₃	Cubic	-1276.20	-1408.90	126.60	37.36	558.2502	-44.302	871657.32	-5615.29	200–350	D98
Tb(OH) ₃	Cubic	-1281.10	-1414.80	128.40	36.49	558.8346	-44.577	1041050	-5623.85	10–350	D98
Dy(OH) ₃	Cubic	-1280.79	-1414.45	130.30	37.98	-	-	-	-	-	-
Ho(OH) ₃	Cubic	-1297.40	-1431.10	130.00	35.84	568.9153	-44.878	1049500	-5771.39	10–350	D98
Er(OH) ₃	Cubic	-1288.14	-1421.80	128.60	35.24	-	-	-	-	-	-
Tm(OH) ₃	Cubic	-1286.60	-1421.10	126.50	34.80	-	-	-	-	-	-
Yb(OH) ₃	Cubic	-1262.90	-1395.50	118.60	34.36	-	-	-	-	-	-
Lu(OH) ₃	Cubic	-1288.54	-1419.01	117.15	33.93	-	-	-	-	-	-
Y(OH) ₃	Cubic	-1304.39	-1438.26	99.20	35.96	575.1682	-46.487	927559.26	-5862.91	10–350	D98
LaCl ₃	UCl ₃	-995.89	-1071.52	137.57	63.90	74.9288	5.1654	684520	-	1133	KK03
CeCl ₃	UCl ₃	-983.61	-1059.02	151.42	62.52	90.9772	3.5812	-271530	-	1090	KK03
PrCl ₃	UCl ₃	-982.72	-1058.77	153.30	61.40	85.6511	3.9524	134650	-	1060	KK03
NdCl ₃	UCl ₃	-965.56	-1041.18	153.43	60.47	87.2834	3.8586	40210	-	1032	KK03
PmCl ₃	UCl ₃	-955.47	-	-	-	-	-	-	-	-	-
SmCl ₃	UCl ₃	-949.55	-1025.32	150.12	59.12	95.3748	3.3444	-516135	-	950	KK03
EuCl ₃	UCl ₃	-855.39	-935.41	144.06	58.50	100.9736	3.0092	-263620	-	894	KK03
GdCl ₃	UCl ₃	-943.28	-1018.20	151.42	58.03	88.7959	3.1444	-34750	-	875	KK03
TbCl ₃	PuBr ₃	-1010.60	-1085.74	154.85	-	86.292	3.8598	-	-	783	KK03
DyCl ₃	AlCl ₃	-923.34	-994.02	175.40	74.38	-34.7111	8.714	-1978460	2265.502	924	KK03
HoCl ₃	AlCl ₃	-928.29	-997.68	177.10	74.80	100.382	0.5091	-	-	993	KK03
ErCl ₃	AlCl ₃	-925.02	-994.81	175.10	75.21	-28.255	8.272	-2055060	2177.088	1049	KK03
TmCl ₃	AlCl ₃	-926.20	-996.09	173.50	75.59	-38.3601	8.67	-2308450	2382.415	1095	KK03
YbCl ₃	AlCl ₃	-892.36	-959.51	169.30	76.04	-55.7145	9.322	-2731060	2752.211	1138	KK03
LuCl ₃	AlCl ₃	-917.76	-987.12	153.00	76.31	-74.5384	10.439	-3070270	3000.228	1198	KK03

YCl ₃	AlCl ₃	-940.90	-1013.13	136.82	74.83	101.7423	0.715464	-1051439	-	298–994	P84
LaF ₃	LaF ₃	-1656.37	-1732.05	106.98	-	-329.312	16.191	15085500	9212.611	1766	KK03
CeF ₃	LaF ₃	-1641.37	-1718.50	115.23	-	-59.1137	8.063	-4575500	3075.152	1703	KK03
PrF ₃	LaF ₃	-1641.37	-1717.91	121.22	-	14.00406	3.548	-5381370	2197.807	1670	KK03
NdF ₃	LaF ₃	-1634.37	-1710.64	120.79	-	37.82125	4.02	-2617590	1231.834	1649	KK03
SmF ₃	YF ₃	-1624.37	-1701.09	116.50	-	169.0564	-7.6809	-4840760	-	743	KK03
EuF ₃	YF ₃	-1544.55	-1625.63	110.07	-	117.4275	-	-1735890	-	973	KK03
GdF ₃	YF ₃	-1621.37	-1698.14	114.77	-	102.3403	0.60945	-1401620	-	1347	KK03
TbF ₃	YF ₃	-1618.37	-1695.14	118.97	-	97.5769	1.98845	-1156100	-	1446	KK03
DyF ₃	YF ₃	-1616.87	-1695.57	118.07	-	107.776	1.763	-586828.7	-299.813	1426	KK03
HoF ₃	YF ₃	-1624.37	-1701.61	120.34	-	-98.1651	8.272	-7160320	4159.99	1416	KK03
ErF ₃	YF ₃	-1614.37	-1692.45	116.86	-	6.16555	4.455	-4469530	2073.427	1388	KK03
TmF ₃	YF ₃	-1614.37	-1692.63	114.98	-	53.9644	2.401	-3044090	1097.046	1325	KK03
YbF ₃	YF ₃	-1587.37	-1662.58	111.84	-	103.7012	0.92366	-1516080	-	1267	KK03
LuF ₃	YF ₃	-1610.37	-1688.00	94.83	-	89.0368	1.92857	-685980	-	1230	KK03
YF ₃	YF ₃	-1632.86	-1710.36	88.70	-	106.8418	0.16485	-434000	-	298–1350	P84
LaFeO ₃	Perovskite	-1277.80	-1351.2	118.00	-	-	-	-	-	-	-
CeFeO ₃	Perovskite	-1274.59	-	-	-	-	-	-	-	-	-
PrFeO ₃	Perovskite	-1282.00	-1364.6	102.70	57.48	-	-	-	-	-	-
NdFeO ₃	Perovskite	-1277.40	-1359.9	116.00	57.26	-	-	-	-	-	-
SmFeO ₃	Perovskite	-1284.10	-1367	161.50	-	-	-	-	-	-	-
EuFeO ₃	Perovskite	-1194.50	-1280.6	188.00	-	-	-	-	-	-	-
GdFeO ₃	Perovskite	-1269.80	-1365.3	129.00	-	-	-	-	-	-	-
TbFeO ₃	Perovskite	-1282.19	-1383.9	65.91	-	-	-	-	-	-	-
DyFeO ₃	Perovskite	-1285.30	-1378.8	126.80	-	-	-	-	-	-	-
HoFeO ₃	Perovskite	-1289.10	-1388.7	131.00	-	-	-	-	-	-	-
ErFeO ₃	Perovskite	-1287.80	-1397.1	137.10	-	-	-	-	-	-	-
TmFeO ₃	Perovskite	-1286.96	-	86.00	-	-	-	-	-	-	-
YbFeO ₃	Perovskite	-1261.20	-1354.3	82.44	-	-	-	-	-	-	-
LuFeO ₃	Perovskite	-	-1385.6	-	-	-	-	-	-	-	-

YFeO ₃	Perovskite	-1296.40	-	-	-	-	-	-	-	-	-
La ₂ (CO ₃) ₃	-	-3141.77	-3378.05	261.08	-	-	-	-	-	-	-
Ce ₂ (CO ₃) ₃	-	-3120.57	-3357.69	284.51	-	-	-	-	-	-	-
Pr ₂ (CO ₃) ₃	-	-3130.57	-3369.34	287.02	-	-	-	-	-	-	-
Nd ₂ (CO ₃) ₃	-	-3113.40	-3349.75	292.46	-	-	-	-	-	-	-
Pm ₂ (CO ₃) ₃	-	-3100.89	-	-	-	-	-	-	-	-	-
Sm ₂ (CO ₃) ₃	-	-3102.02	-3338.95	284.93	-	-	-	-	-	-	-
Eu ₂ (CO ₃) ₃	-	-2910.50	-3153.69	280.33	-	-	-	-	-	-	-
Gd ₂ (CO ₃) ₃	-	-3097.75	-3333.89	284.51	-	-	-	-	-	-	-
Tb ₂ (CO ₃) ₃	-	-3106.07	-3343.95	287.02	-	-	-	-	-	-	-
Dy ₂ (CO ₃) ₃	-	-3093.23	-3335.43	283.68	-	-	-	-	-	-	-
Ho ₂ (CO ₃) ₃	-	-3123.16	-3361.30	292.04	-	-	-	-	-	-	-
Er ₂ (CO ₃) ₃	-	-3110.11	-3348.97	288.28	-	-	-	-	-	-	-
Tm ₂ (CO ₃) ₃	-	-3110.16	-3352.64	273.63	-	-	-	-	-	-	-
Yb ₂ (CO ₃) ₃	-	-3050.55	-3287.05	266.94	-	-	-	-	-	-	-
Lu ₂ (CO ₃) ₃	-	-3105.73	-3343.78	243.93	-	-	-	-	-	-	-
Y ₂ (CO ₃) ₃	-	-3148.04	-3385.43	233.05	-	-	-	-	-	-	-
La ₂ (CO ₃) ₃ ·8H ₂ O	-	-4958.88	-5688.65	471.96	-	-	-	-	-	-	-
Ce ₂ (CO ₃) ₃ ·8H ₂ O	-	-4958.04	-5670.43	556.47	-	-	-	-	-	-	-
Pr ₂ (CO ₃) ₃ ·8H ₂ O	-	-4947.16	-5699.38	430.95	-	-	-	-	-	-	-
Nd ₂ (CO ₃) ₃ ·8H ₂ O	-	-4931.26	-	-	-	-	-	-	-	-	-
Sm ₂ (CO ₃) ₃ ·3H ₂ O	-	-3739.24	-4521.43	322.17	-	-	-	-	-	-	-
Eu ₂ (CO ₃) ₃ ·3H ₂ O	-	-3553.89	-4356.07	271.54	-	-	-	-	-	-	-
Gd ₂ (CO ₃) ₃ ·3H ₂ O	-	-3728.78	-4510.92	319.24	-	-	-	-	-	-	-
Tb ₂ (CO ₃) ₃ ·3H ₂ O	-	-3736.78	-4528.28	296.23	-	-	-	-	-	-	-
Dy ₂ (CO ₃) ₃ ·3H ₂ O	-	-3732.13	-4509.73	353.97	-	-	-	-	-	-	-
Ho ₂ (CO ₃) ₃ ·3H ₂ O	-	-3748.03	-4522.57	358.99	-	-	-	-	-	-	-
Er ₂ (CO ₃) ₃ ·3H ₂ O	-	-3736.31	-4510.58	358.57	-	-	-	-	-	-	-
Tm ₂ (CO ₃) ₃ ·3H ₂ O	-	-3719.58	-4483.86	389.53	-	-	-	-	-	-	-
Yb ₂ (CO ₃) ₃ ·6H ₂ O	-	-4389.02	-	-	-	-	-	-	-	-	-
Lu ₂ (CO ₃) ₃ ·6H ₂ O	-	-4356.38	-	-	-	-	-	-	-	-	-

$Y_2(CO_3)_3 \cdot 3H_2O$ - -3766.87 -4539.03 305.43 - - - - - - -

Abbreviations: K14: [Konings et al. \(2014\)](#); MK05: [Morss and Konings \(2004\)](#); D98: [Diakonov et al. \(1998\)](#); KK03: [Konings and Kovács \(2003\)](#); P84: [Pankratz \(1984\)](#).

Figures

Figure 1

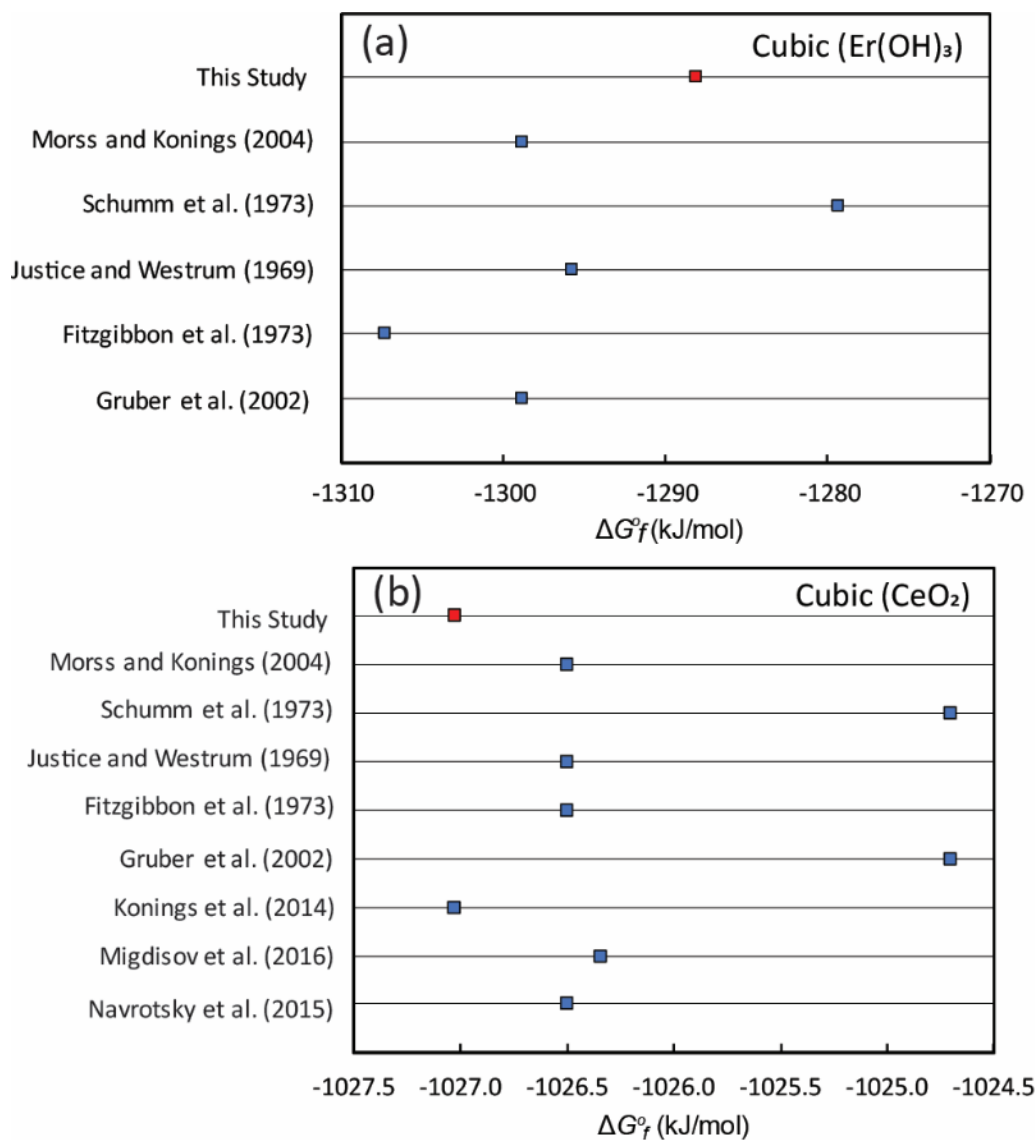


Figure 1. Examples of the ΔG_f° scatter in the literature at 25 °C and 1 bar for REE crystalline solids. (a) Cubic Er(OH)_3 and (b) Cubic CeO_2 crystalline solids. All cited dark symbols are calorimetric measurements.

Figure 2

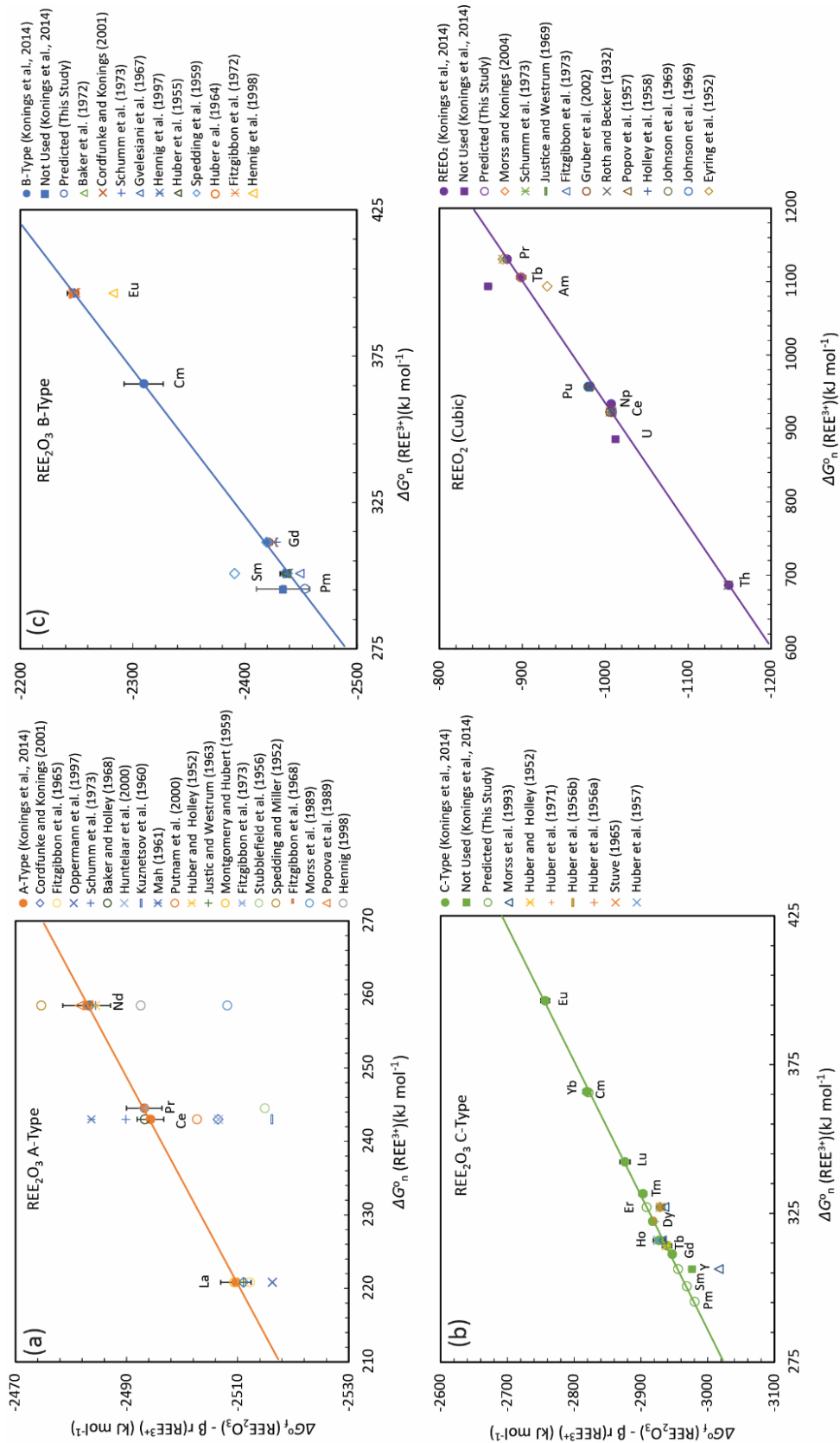


Figure 2. Graphical representations of linear correlations of isostructural (a) A-Type REE₂O₃, (b) B-Type REE₂O₃, (c) C-Type REE₂O₃, and (d) cubic REEO₂ mineral families and comparisons with previous studies. Solid circles represent the experimental data used for regression. Solid squares are experimental data not used in regression. Filled circles stand for calorimetry data and other symbols of solubility data. Predicted values show as open circles.

Figure 3

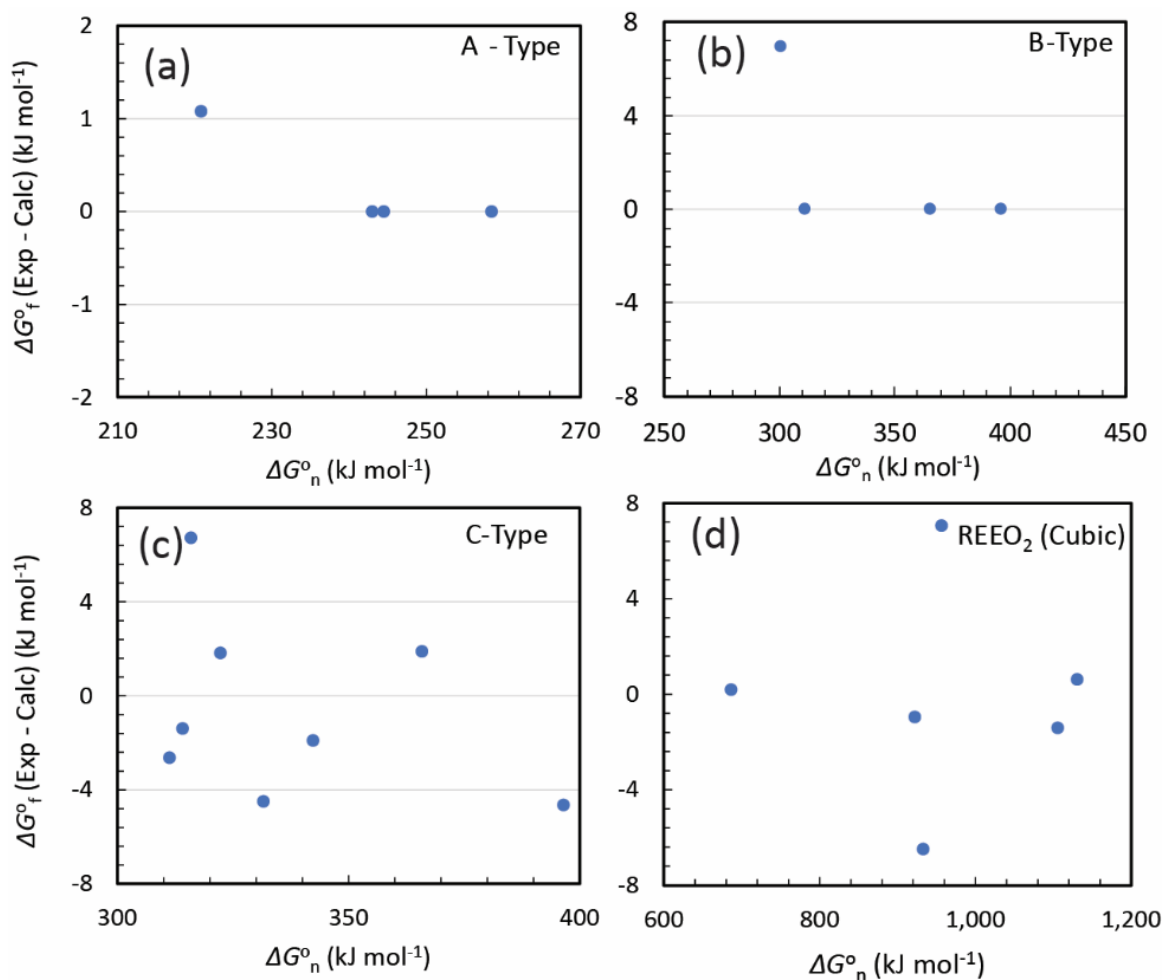


Figure 3. Residuals between the experimentally measured and calculated ΔG_f^0 values of the crystalline solids from the four isostructural mineral families. **(a)** A-Type REE₂O₃, **(b)** B-Type REE₂O₃, **(c)** C-Type REE₂O₃, and **(d)** cubic REEO₂.

Figure 4

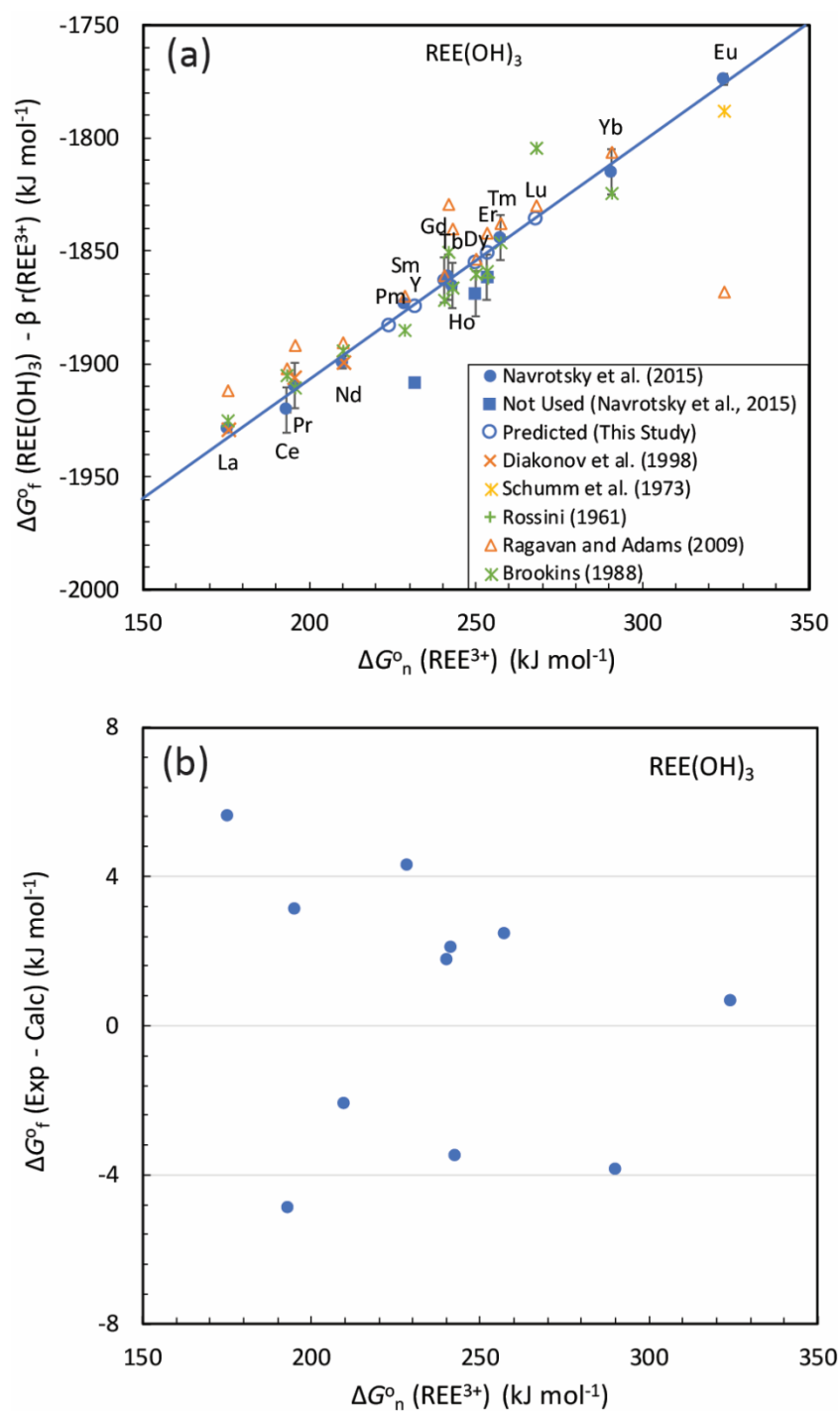


Figure 4. (a) Graphical representations of linear correlations of isostructural REE(OH)₃ mineral families and comparisons with previous studies, and (b) Residuals between the experimentally measured and calculated ΔG_f° values for REE(OH)₃ isostructural family. Solid circles are used in regressions and solid squares are not used in regression. Bars represent the uncertainties of ΔG_f° values.

Figure 5

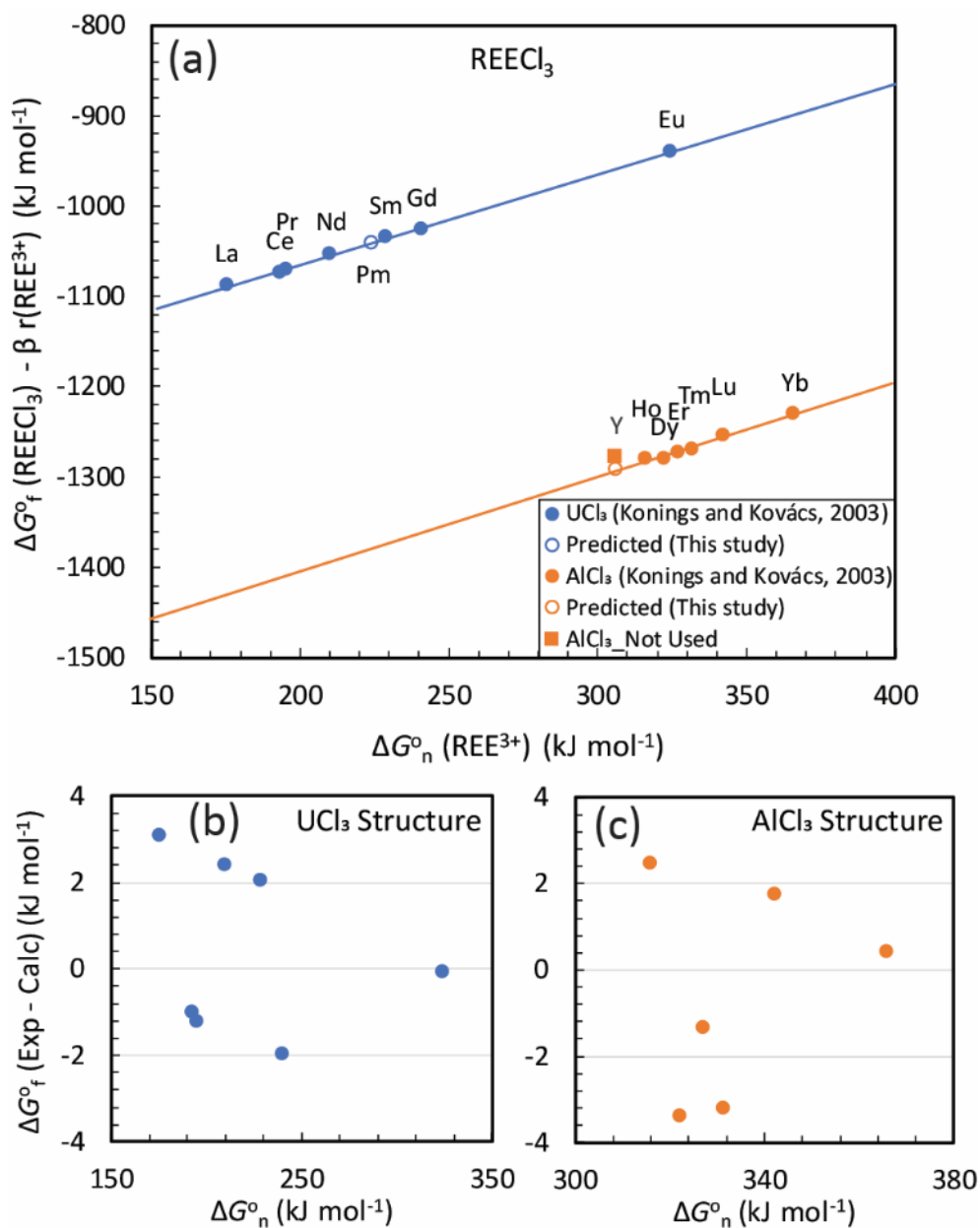


Figure 5. (a) Graphical representations of linear correlations of isostructural REECl₃ mineral families (UCl₃ and AlCl₃ structures), and (b) Residuals between the experimentally measured and calculated ΔG°_f values for REECl₃ isostructural family.

Figure 6

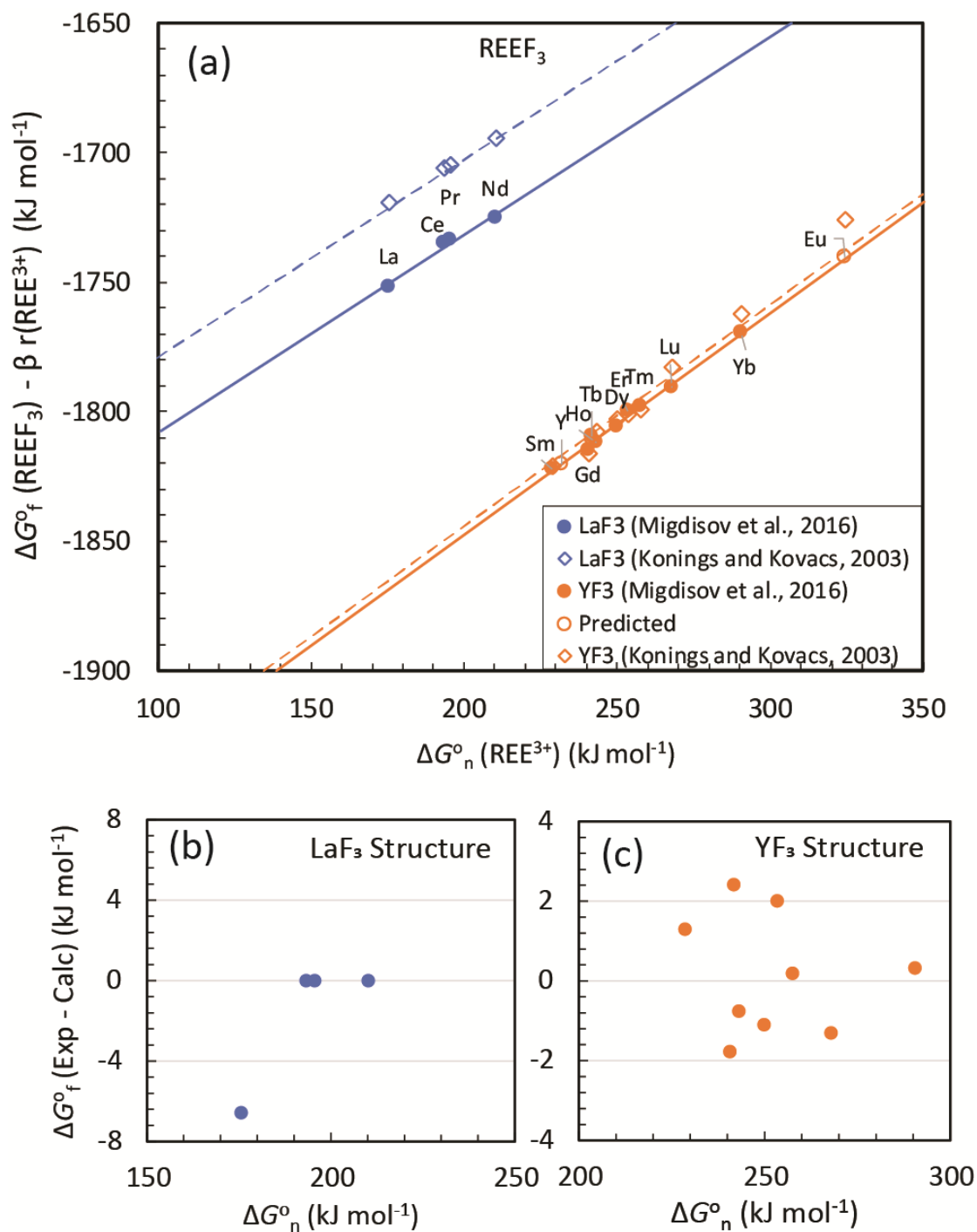


Figure 6. (a) Graphical representations of linear correlations of isostructural REEF₃ mineral families (LaF₃ and YF₃ structures) and comparisons with previous calorimetry studies [Konings and Kovács \(2003\)](#), and (b-c). Residuals between the experimentally measured and calculated ΔG_f° values for REEF₃ isostructural family. Filled circles denote the data from mineral solubility experiments from [Migdisov et al. \(2016\)](#), and open diamonds denote the calorimetric measurements from [Konings and Kovács \(2003\)](#).

Figure 7

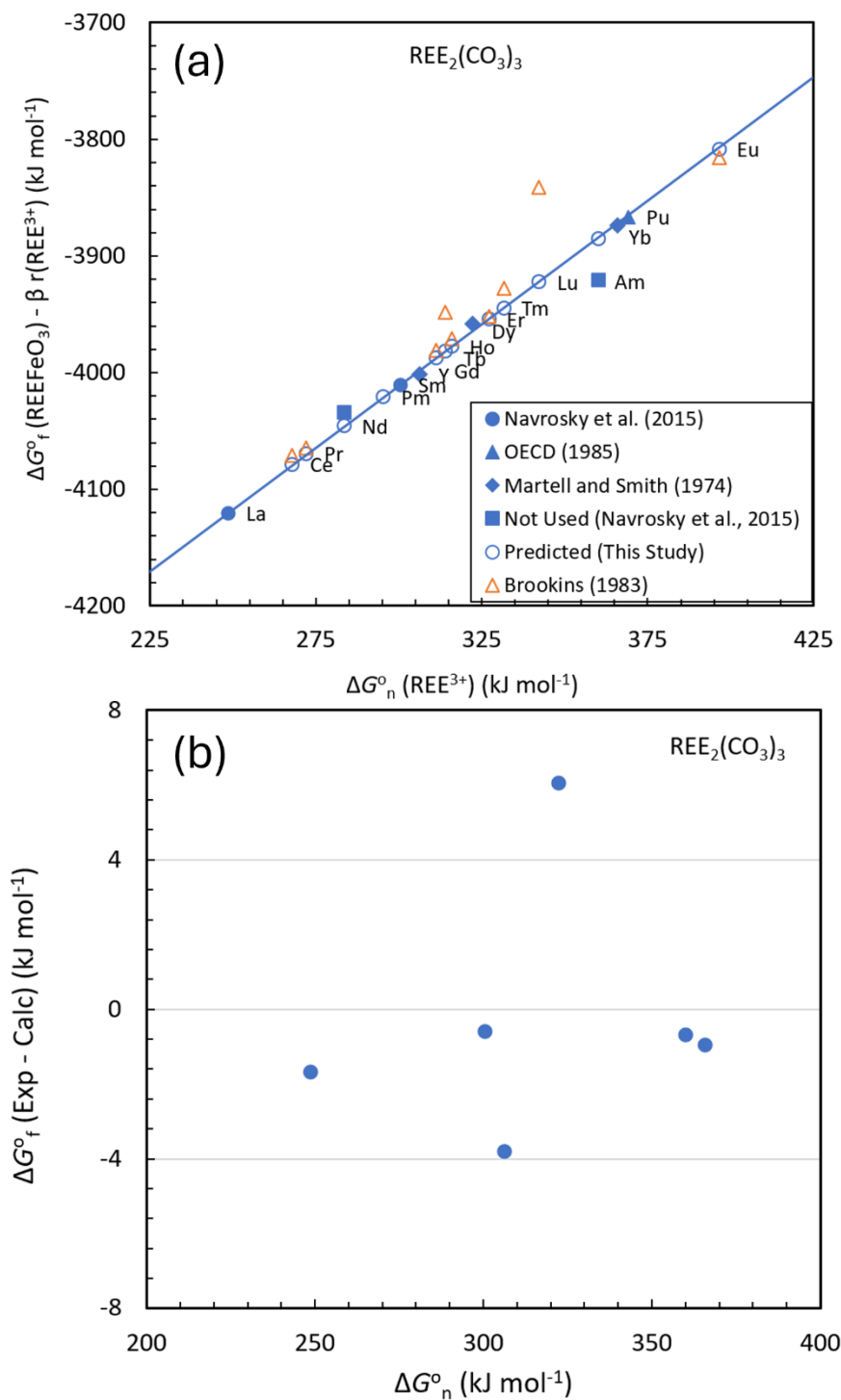


Figure 7. (a) Graphical representations of linear correlations of isostructural $\text{REE}_2(\text{CO}_3)_3$ mineral families and comparisons with previous studies (Brookins, 1988; Martell and Smith, 1974; Navrotsky et al., 2015; OECD, 1985), and (b) Residuals between the experimentally measured and calculated ΔG_f° values for $\text{REE}_2(\text{CO}_3)_3$ isostructural family.

Figure 8

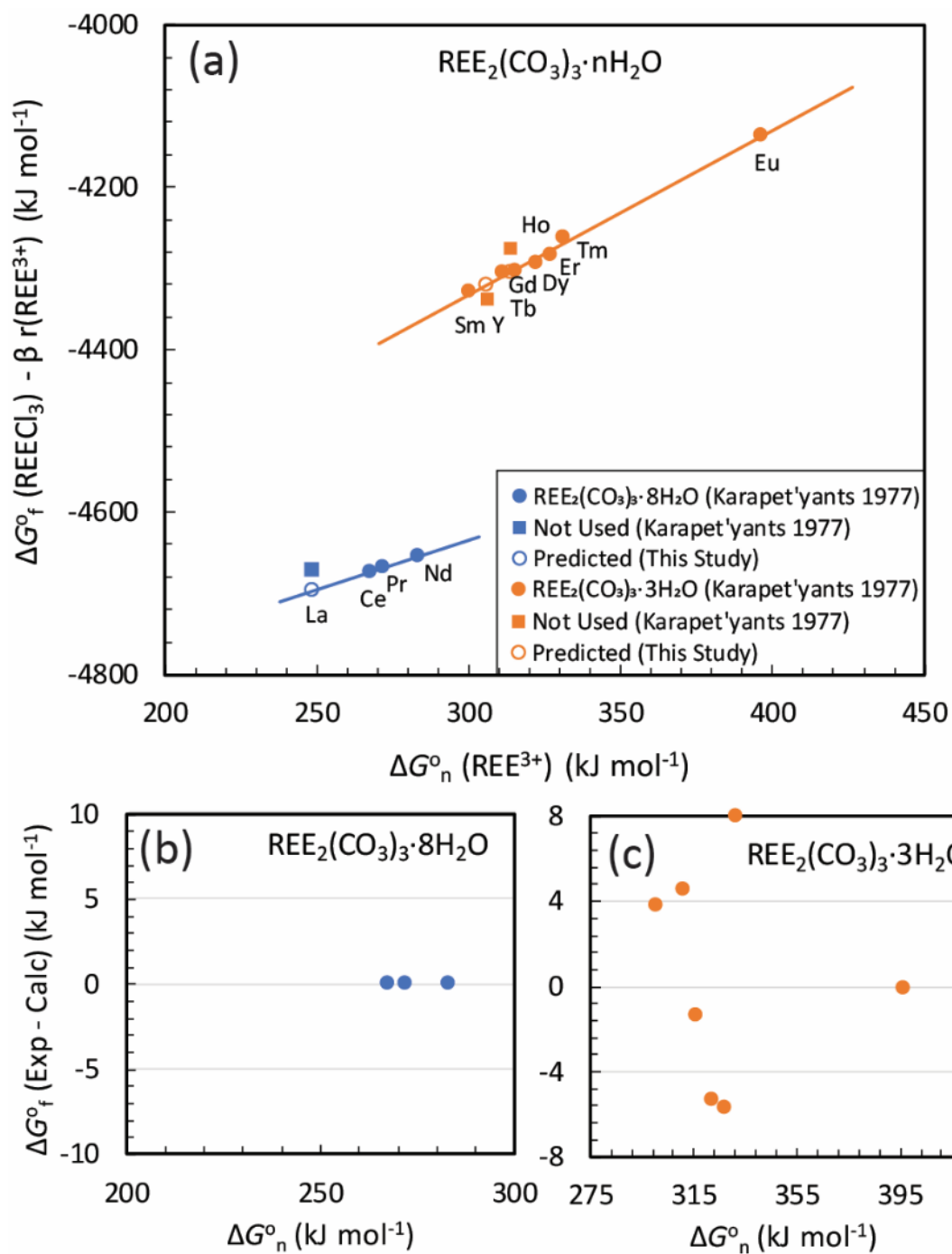


Figure 8. (a) Graphical representations of linear correlations of isostructural REE₂(CO)₃·nH₂O mineral families, and residuals between the originally reported in Karapet'yants et al. (1977) and calculated ΔG°_f values for (b) REE₂(CO)₃·8H₂O and (c) REE₂(CO)₃·3H₂O isostructural family.

Figure 9

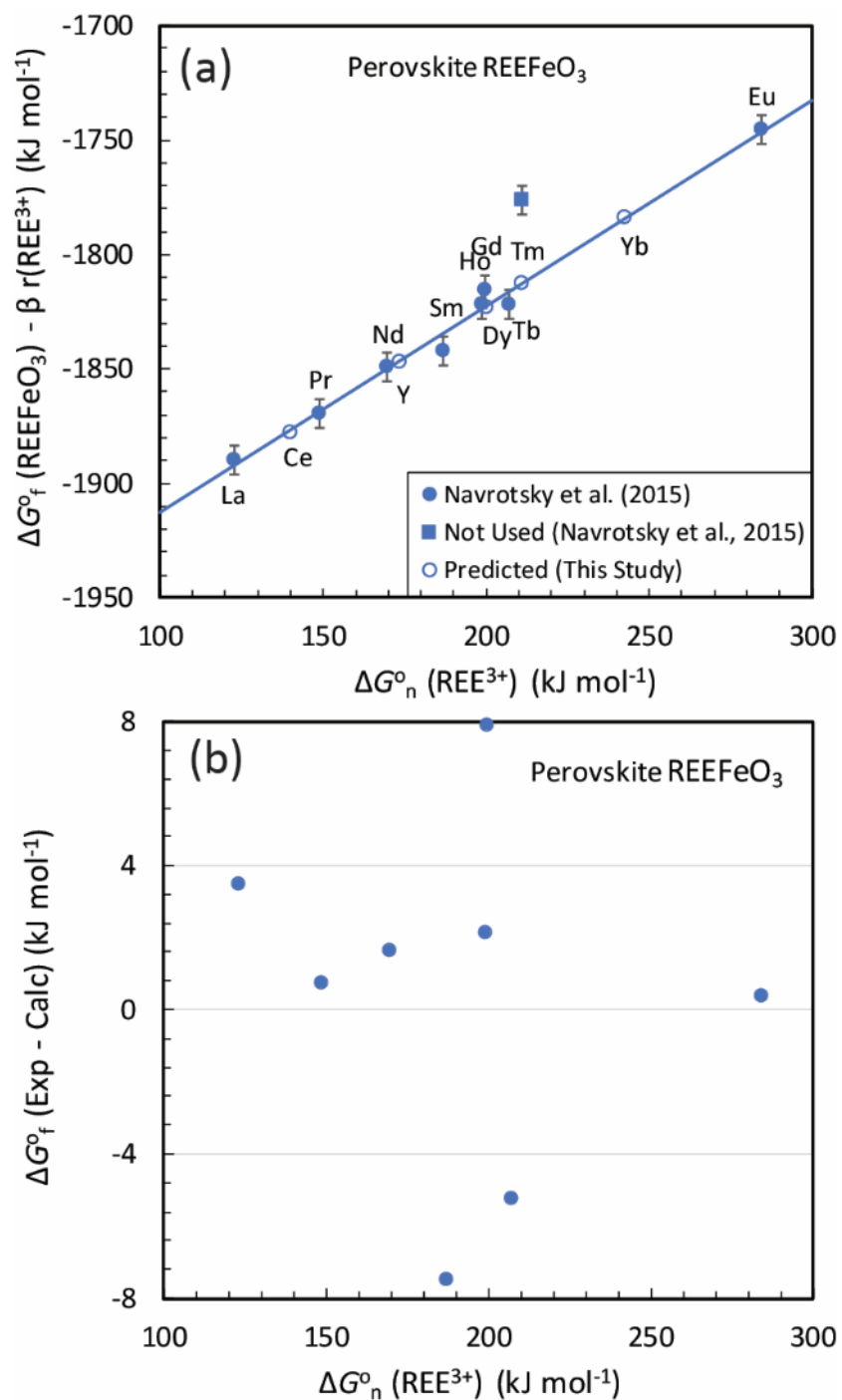


Figure 9. (a) Graphical representations of linear correlations of isostructural perovskite REEFeO₃ mineral families, and (b) Residuals between the experimentally measured and calculated ΔG_f° values for perovskite REEFeO₃ isostructural family.

Figure 10

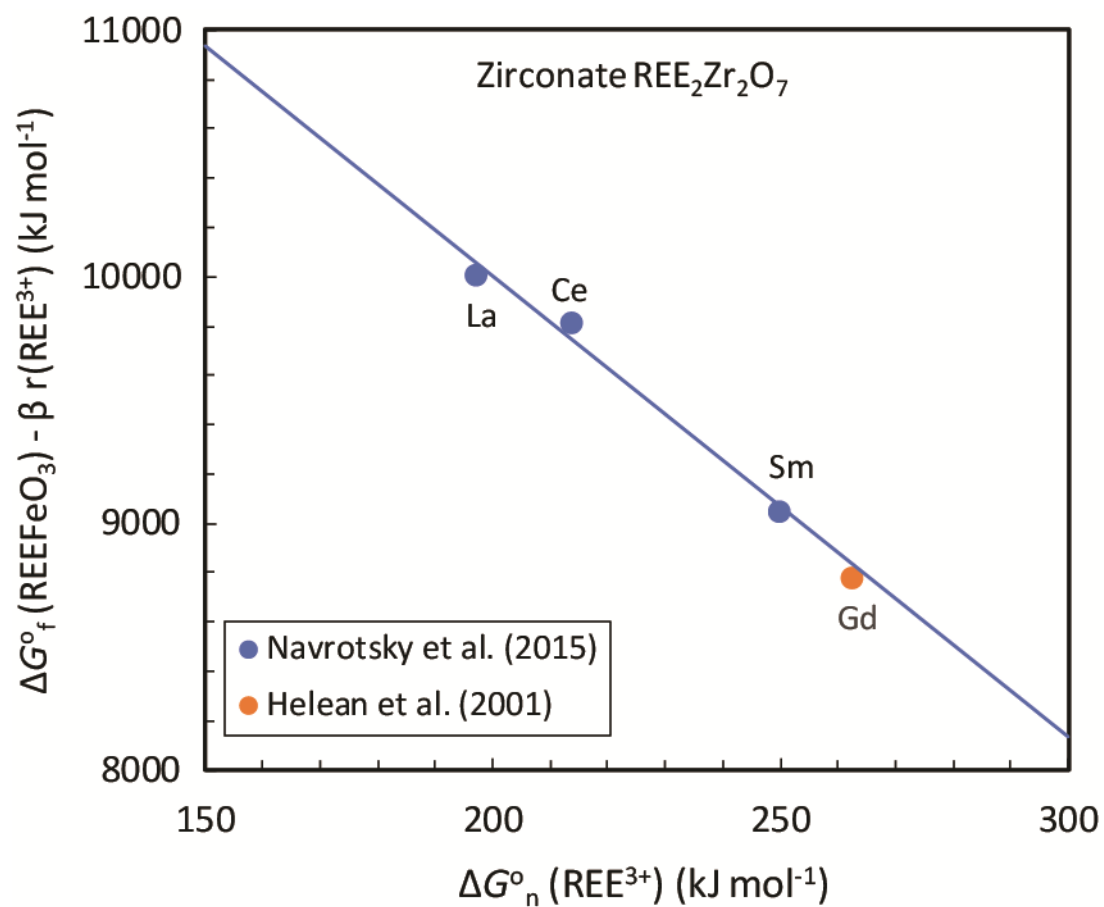


Figure 10. Graphical representations of linear correlations of isostructural zirconate $\text{REE}_2\text{Zr}_2\text{O}_7$ mineral families. Only the $\text{Gd}_2\text{Zr}_2\text{O}_7$ data is from Helean et al. (2000) to construct the linear correlation. The negative slope indicates that the selected dataset for zirconate is not recommended.

Figure 11

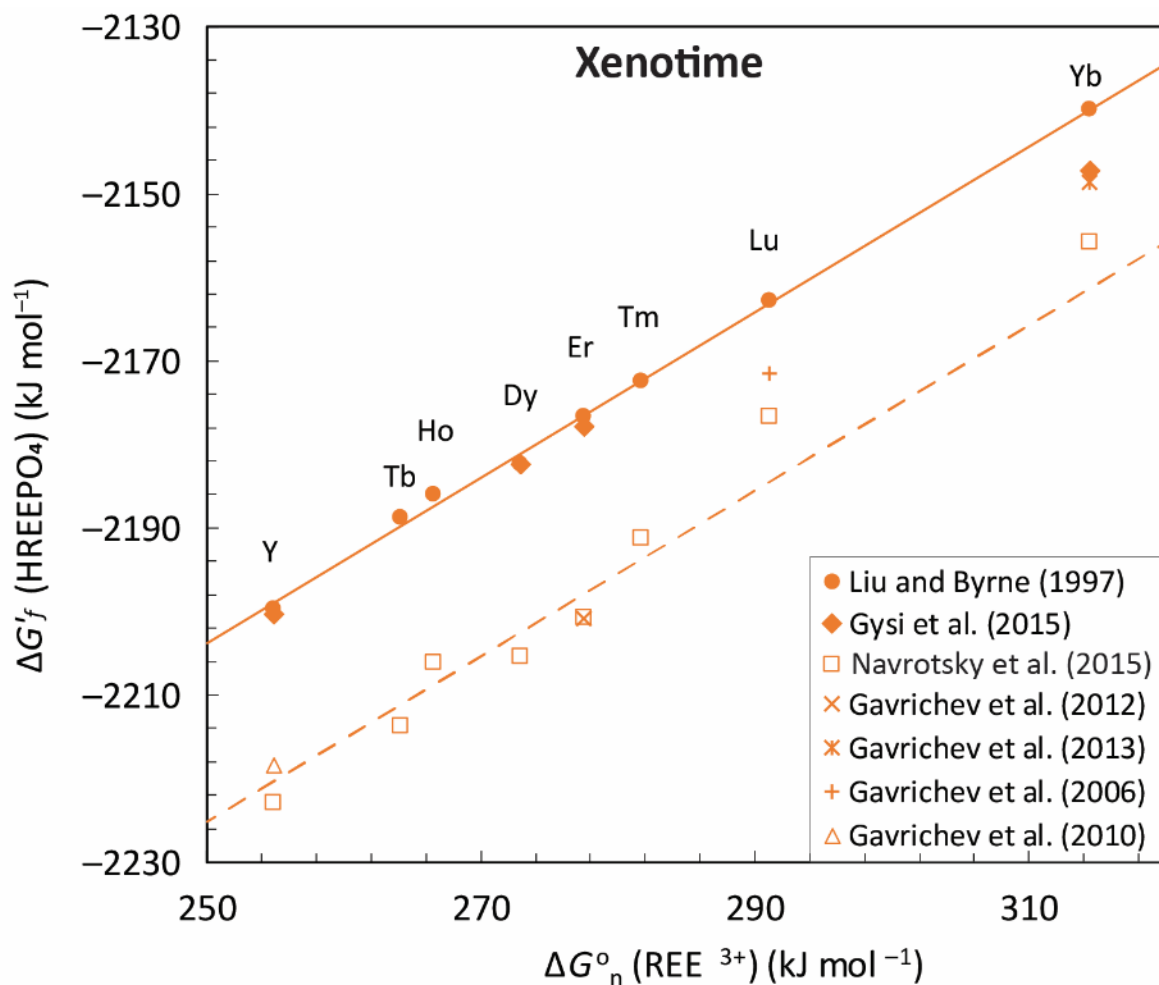


Figure 11. Graphical representations of linear correlations of isostructural xenotime and comparisons with other experimental studies (Gavrichev et al., 2013; Gavrichev et al., 2012; Gavrichev et al., 2010; Gavrichev et al., 2006; Gysi et al., 2015; Liu and Byrne, 1997; Navrotsky et al., 2015). Solid symbols represent mineral solubility experiments and open symbols represent calorimetric experiments.

Figure 12

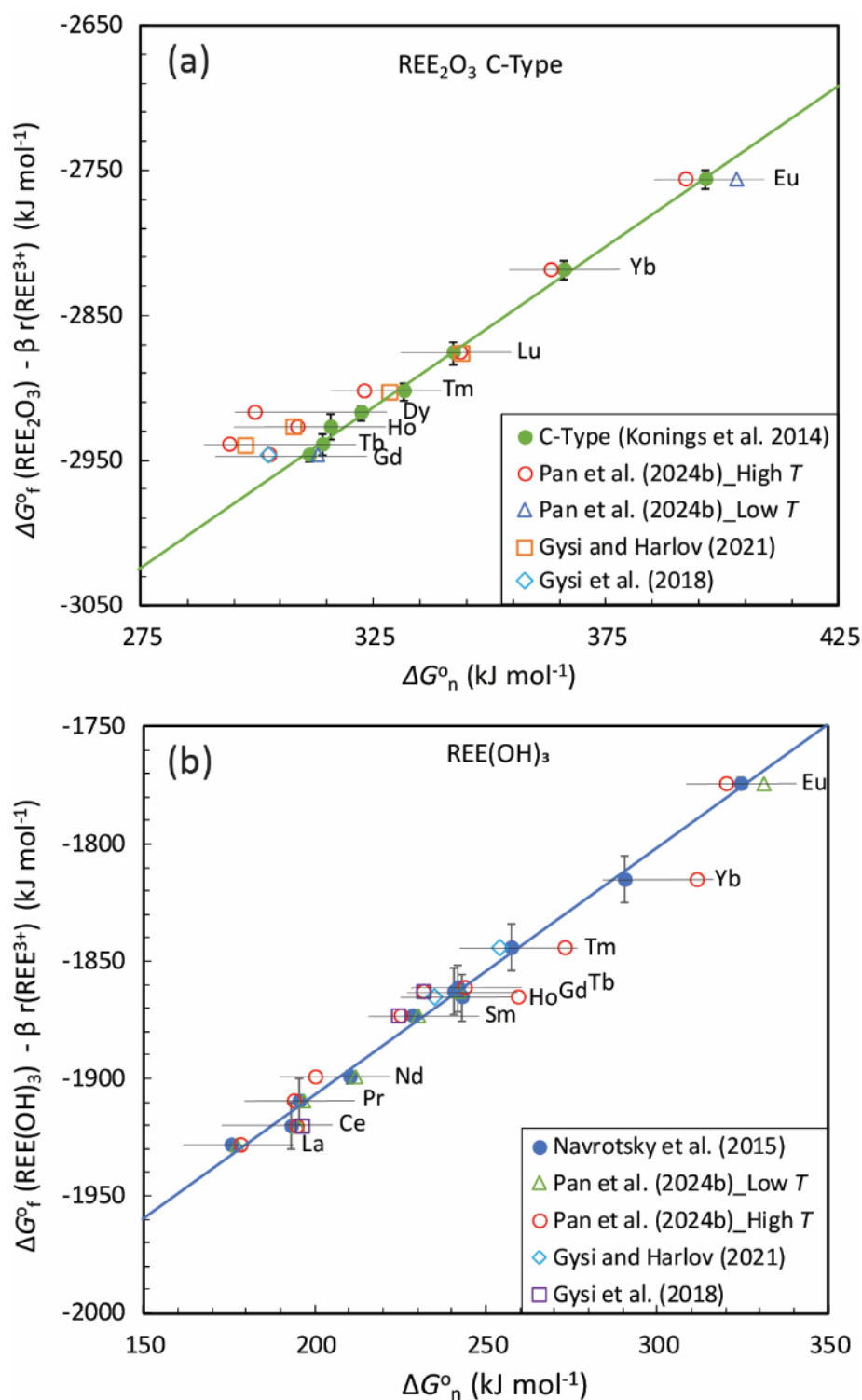


Figure 12. Linear correlations of (a) REE₂O₃ C-Type and (b) REE hydroxides constructed with the REE³⁺ from Shock et al. (1997) and comparisons with previously reported ΔG°_f values in literature (Gysi and Harlov, 2021; Gysi et al., 2018; Konings et al., 2014; Pan et al., 2024b).



Click here to access/download
Supplementary Material
Appendix A.pdf

